CHARACTERIZATION OF THERMAL AND EPITHERMAL NEUTRON SPECTRA

A Thesis Submitted for the Award of the Degree of Doctor of Philosophy of the University of London

by

STUART MARK JEFFERIES

The Reactor Centre

Department of Mechanical Engineering

Imperial College of Science and Technology

Silwood Park

Ascot

Berkshire.

December 1982

PRO EIS QUŌS AMO

ABSTRACT

The purpose of this work is to measure and evaluate the thermal and epithermal neutron activation data for the thermal and epithermal neutron standard flux facilities at the National Physical Laboratory (Middlesex, England), including the 2200 ms^{-1} activation cross-sections, the resonance activation integrals and decay data for the neutron capture products.

These are the data required for routine metrology, activation analysis and calculations of activation in reactor materials.

This work includes:

(1) A detailed investigation into high-resolution gamma-ray spectroscopy with a special emphasis on analytical spectrum fitting, pulse pile-up, coincidence summing effects and the generation of precise efficiency curves. The final technique which evolved from the investigation was tested by using a set of sources provided by the I.A.E.A. for their "G-2 Intercomparison of High Precision Gamma-ray Spectroscopy". The results which were obtained equalled the best entered for the intercomparison.

(2) A description of two Monte-Carlo codes which can be used for the calculation of thermal and resonance self-shielding factors. These factors are important when using thick foils for activation measurements.

(3) A description of a neutron flux convention used to characterize the thermal and epithermal neutron fluxes in an irradiation facility and the use of a generalised least-squares technique, which from measured reaction rates, determines best values of the flux parameters and also provides improved estimates of the nuclear data included in the calculation.

(4) Use of this new flux convention in the calibration of the N.P.L. thermal and epithermal neutron standard flux facilities. The results from the epithermal neutron flux facility calibration are consistent with the assumption that the flux is proportional to 1/E in this facility.

(5) A comparison of nuclear data obtained in this work with published literature values.

ACKNOWLEDGEMENTS

It gives me great pleasure to thank my supervisors, Desmond MacMahon and Bruno Ryves not only for their invaluable advice and constant encouragement throughout, but also for making it a pleasure to do this work.

Special thanks go to John Williams and Peter Gray for their useful suggestions and untiring disposition in answering questions at all times, and Peter Kolkowski and Roy Johnson for their patience and help in the experimental aspects of this work.

19th November 1982

TABLE OF CONTENTS

LIST OF TABLES

LIST OF FIGURES

CHAPTER ONE

INTRODUCTION

In the characterization of thermal and epithermal neutron fields the assumption has often been made that the neutron flux distribution can be represented by a Maxwellian thermal component and an epithermal slowing down spectrum proportion to 1/E. The neutron flux conventions of Westcott ([1], Stoughton and Halperin ([2], and Hogdahl ([3] all make use of this assumption. However, a 1/E slowing down spectrum arises in systems in which the slowing down density is constant and can only be expected in the absence of the effects of leakage and absorption. For most practical sources of neutron spectra, the epithermal component will deviate from the 1/E form normally assumed. It has been shown by Williams ([4] that in the case of energy independent buckling and absorption cross-section the flux per unit energy is approximately proportional to $1/E^{1+\alpha}$. Functions containing this type of deviation from the 1/E spectrum have also been proposed on empirical grounds by many authors ([5-9]. In the flux conventions cited above, the reaction rate for a radiative capture reaction, in which the fast neutron contribution is negligible, depends on the effective thermal cross-section and on the resonance integral, defined here as:

$$I_o = \int_{E_{Cd}}^{\infty} \sigma(E)\, E^{-1}\, dE$$

where E_{Cd} is the effective cut-off energy of a cadmium box. Resonance integrals are important data which are required in fields such as experimental reactor physics, dosimetry, neutron standardization,

epithermal-neutron-activation-analysis and measurement of neutron slowing-down spectra. They are also used in checking nuclear resonance parameters. However, the recent compilation of resonance integrals by Gryntakis and Kim ([10] shows, for most isotopes, a very large scatter even in the recent data. It is not unusual to discover that several measured values of the same isotope may differ from one another by more than the standard deviations claimed by each individual measurement. Since it has been shown ([5,6,8] that deviations from the commonly assumed 1/E shaped epithermal spectrum can lead to severe changes in the apparent resonance integral; it is believed that the scatter in the data is mainly due to a failure of the measurers to determine the shape of the epithermal spectrum in which the resonance integrals were measured.

It is also believed that part of the scatter is due to systematic errors arising from some negligence in the experiments. For example, effects such as neutron self-shielding and gamma self-absorption in the detector foil are often ignored. If reliable resonance integral data are to be produced, the importance of being able to characterize neutron spectra very carefully, is self evident.

Ahmad ([11] has proposed a neutron flux convention in which the neutron flux distribution is described in terms of three parameters, and any deviations from a 1/E spectrum are assumed to be of the form $1/E^{1+\alpha}$. The validity of this new flux convention has been tested ([11] with activation data from several laboratories and has so far proved to be reliable. This work uses this new flux convention in the evaluation of activation data measured in the standard thermal and epithermal neutron flux facilities at the National Physical Laboratory (Middlesex,

England). The purpose of the experiments described in chapters four and five was to primarily calibrate the two standard facilities in terms of the three flux parameters mentioned above. The best method of estimating these flux parameters is one which requires more measured quantities than the minimum in order to produce an over-determined set of simultaneous equations. The best-values for the flux parameters can then be obtained by applying a generalized least squares approach. If the nuclear parameters which appear in the equation relating the measured reaction-rate to the three flux parameters, are not treated as constants; then it is also possible to gain improved knowledge of the nuclear parameters from the same activation data used to determine the flux parameters. This approach is logical since the estimated accuracies of the nuclear parameters, particularly the resonance integral cross-sections, are often poorer than those of the measured reaction-rates. Ignoring the cross-section uncertainties by treating them as constants would significantly affect the estimated uncertainties in the flux parameters.

This work, therefore, also includes new information on some of the nuclear data which was required for the evaluation of the measured activations.

One of the greatest practical problems which arises in this type of work is in the measurement of resonance self-shielding. In neutron fluxes greater than 10^{15} neutrons/m^2/sec., it is usually possible to use foil detectors which are sufficiently thin or dilute that any self-shielding effects are negligible. It is frequently necessary, however, to make measurements in much lower fluxes, for example in standard facilities. It is then necessary to use relatively thick foils in which

self-shielding factors are important. Although these factors have been studied previously by several authors (see Chapter three), there are still many detector materials for which the literature contains no precise data. Even when literature values are available it is not always evident how they should be applied, because of two conflicting definitions which are in use.

Chapter three of this work describes the use of a Monte-Carlo code for the calculation of self-shielding factors and recommends the way in which they should be applied.

Throughout this work use is made of the (n,γ) reaction. The methods of detection employed being high-resolution Ge(Li) γ-ray spectroscopy and $4\pi\beta$-γ coincidence counting.

Use of this reaction coupled with high resolution Ge(Li) γ-ray spectroscopy is also commonly used in multi-element analysis for the determination of sub-ppm concentrations.

Chapter two gives the results of a detailed investigation into γ-ray spectroscopy and recommends an experimental procedure which can be used to give results of high accuracy and precision. Chapter six summarizes the results obtained in this work and draws the final conclusions.

CHAPTER TWO

GAMMA-RAY SPECTROSCOPY

In order to make precise and accurate determinations of gamma-ray intensities using Ge or Ge(Li) detectors, several factors must be examined critically. These factors include: (a) an awareness of the capabilities and limitations of the components of the system and the methods used for their optimization; (b) the determination of the net peak area (N.P.A.) under the gamma-ray peak of interest; (c) the application of various correction terms (i.e. for deadtime, pulse pile-up, etc.); (d) the determination of the photopeak efficiency for any gamma-ray in the energy region of interest.

For each of the above factors (a) - (d), the literature was reviewed and various methods (often modified) for measurements and analysis, were selected for the final technique. The validity of this technique was tested using a set of sources provided by the I.A.E.A. for their "Intercomparison of High Precision Gamma-Ray Spectrometry (G-2)."

2.1.1 Peak Area Determination

There are two main methods of determining peak areas, one being the simple net area (S.N.A.) procedure of summing the actual data points between two boundaries and subtracting some form of background function, the other is by using an analytical approximation to the gamma-ray peak shape and integrating the area under the function. In both cases the value which is obtained for the area will depend upon the functional form used to describe the background and in the latter case, that of the peak as well. Because of this ambiguity in the area of a peak, it becomes essential to analyse all peaks in the same manner if values

are to be compared.

Each method has its advantages and disadvantages. Although both methods can be used for intense well-isolated peaks, any peaks which are close-lying or overlapping make S.N.A. analysis difficult and often impossible. Therefore for overlapping peaks the use of some form of analytical function is necessary.

At high count rates however, the shape of the peak starts to become distorted due to pulse pile-up effects, and if an analytical function is being used to describe the gamma-ray peak, the function may start to become inadequate and any results obtained using it become meaningless.

In order to avoid too many constraints it was decided that both methods of analysis should be available.

2.1.2 The S.N.A. Method

In this method, the value obtained for the area is dependant on the choice of boundaries between which the summation is to take place and the form of the baseline function to be used under the peak.

Several methods for determining the boundaries were studied, including:

(a) A modified Debertin's method ([12]) of defining the peak boundaries to be at $C \pm 4\sigma$. Where C is the peak centroid and σ is a measure of the width of the peak.

(b) Using the first minimum in the data either side of the peak centroid.

(c) Michaelis' method, ([13]) where the lower energy boundary is the point at which the actual spectrum deviates from a straight line fitted to the background arising from multiple Compton

events, and the higher energy boundary is the point where the upper tail of the photopeak reaches a constant number of counts per channel.

When using intense high energy gamma-rays methods (a) and (b) on occasions failed to take the low energy tailing into account. (i.e. the peak area was attenuated). Also, if a lot of low energy tailing occurs, placing the boundaries symmetrically about the peak centroid results in a large region of background on the high energy side of the peak being included in the peak region. This is undesirable as it increases the variance on the N.P.A. Only method (c) was found to be satisfactory on all occasions.

The spectral background in the region of a peak consists of three components; (i) the pulses related to radiation from other sources (e.g. the natural background radiation.); (ii) the pulses from higher energy gamma-rays from the source being measured and (iii) the pulses from the desired gamma-ray but for which enough energy is lost from the sensitive volume of the detector to put the count in the spectral distribution below the peak.

The base line under a peak should be constructed in such a way that the resulting N.P.A. is independent of the above effects.

If the contribution of (i), (ii) and (iii) are small compared to the peak area in the photopeak region then errors in the base-line do not effect either the accuracy or the precision of the intensity measurement. However, if these contributions are not small (e.g. if weak gamma-rays are measured in the presence of strong higher energy gamma-rays) then small errors in the base-line construction may cause large errors in the N.P.A. ([14]

It is assumed that contributions (i) and (ii) can be represented by a low order polynomial (often a linear function). Contribution (iii) however, produces an apparent step in the background under the peak. This is due to the summing of multiple Compton events and the final low energy gamma-ray escaping from the sensitive volume of the detector.

If a detector had infinitely narrow resolution and no tailing, then this would result in a step-function pulse distribution ([15]. Although several forms of step function have been proposed ([15-20] it has been shown that the two best functions are (1) the simple (but discontinuous) step and (2) the simple step folded with a Gaussian noise term. The choice between the two functions is decided on the basis of aesthetics or convenience ([15].

For this work it was decided to fit a simple step function in the following manner: (see Fig. 2.1). Once the peak boundaries are obtained (B_1,B_2), suitable regions adjacent to these are chosen for background determinations (l_1,l_2). These regions usually consist of between 8-16 channels. A weighted linear least-squares fit to a straight line ([21] is then performed on the data in each region. The two straight lines thus obtained are extrapolated to the peak centroid C, and their values at C compared. If the two values are not consistent* with each other, then a step is fitted at the centroid. (Fig. 2.1 (a)).

The value of the N.P.A. is then defined as:

$$\text{N.P.A.} = \sum_{i=B_1}^{i=B_2} C_i - (\text{Area under step})$$

where i = channel number

C_i = number of counts in channel number i

Fig 2.1 FITTING OF THE BACKGROUND UNDER A PHOTOPEAK

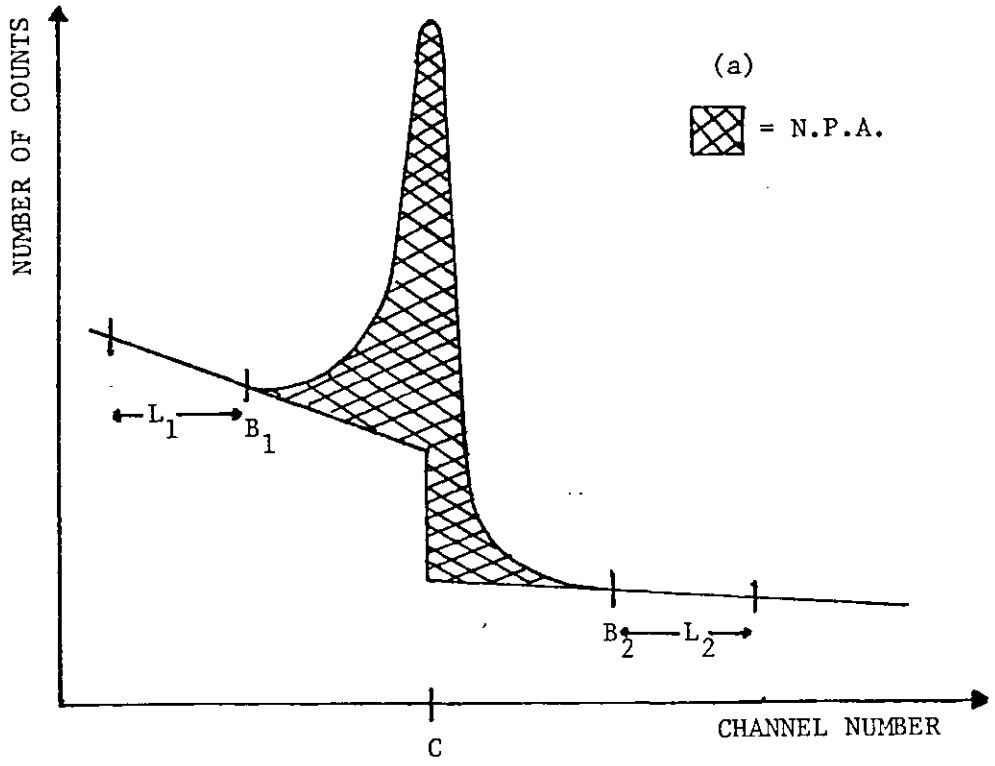

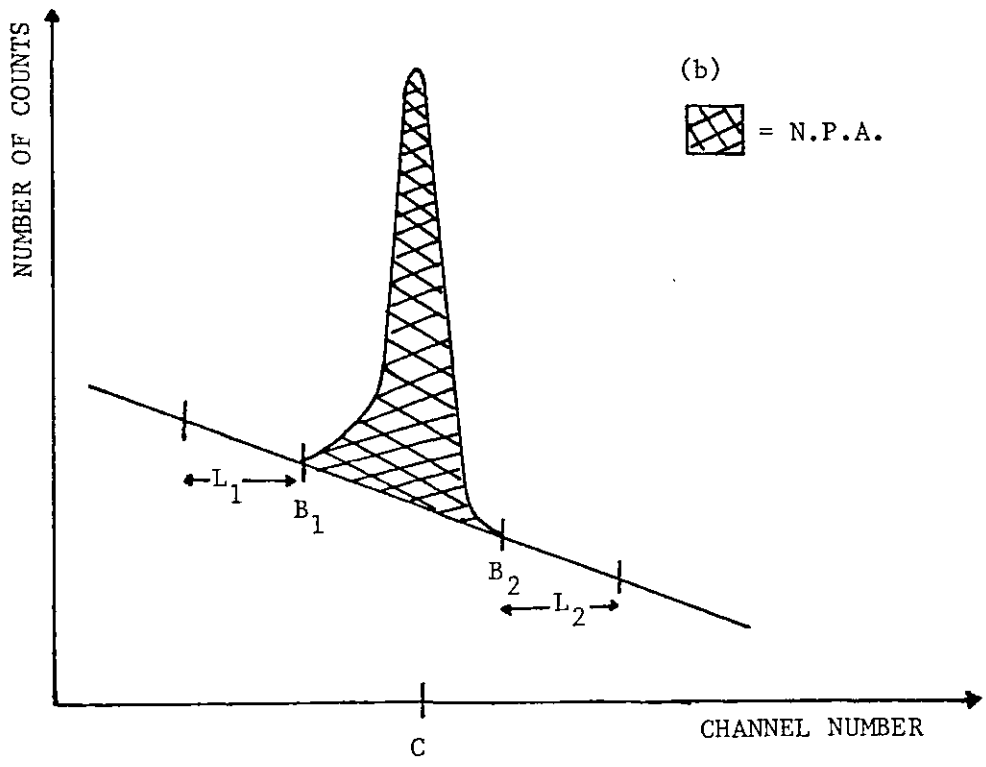

If the two values are consistent* with each other then a step of zero amplitude (i.e. a straight line) is fitted (Fig2.1(b)).

The value of the N.P.A. is then defined as:

$$\text{N.P.A.} = \sum_{i=B_1}^{i=B_2} C_i - (B_2-B_1+1)\left[\frac{\sum_{i=B_1-l_1}^{B_1-1} C_i}{2l_1} + \frac{\sum_{i=B_2+1}^{B_2+l_2} C_i}{2l_2}\right]$$

where l_1, l_2 = number of channels in background interval.

*[The criterion for consistency in this case is defined as $|A-B| \leqslant 4(\sigma_A^2 + \sigma_B^2)^{\frac{1}{2}}$ for two values $A \pm \sigma_A$, $B \pm \sigma_B$]

If $B_2-B_1 = l_1 + l_2$, then the error in the N.P.A. (σ_N) in both cases is assumed to be:

$\sigma_N^2 = T + B$ where T = Total number of counts in peak region

B = Number of background counts

2.1.3 Analytical Fitting of Photopeaks

A wide variety of peak shape functions has been proposed for use in fitting peaks from Ge(Li) detectors ([15-19, 22-25]. A review and comparison of these and several other functions are given in refs.15 and 48.

The shapes which seem to fit the data best of all have a Gaussian peak with the addition of a skewed term or tailing on the low energy side, plus a long tail or step below the peak. Program HYPERMET ([19]was chosen for this work because of the semi-empirical approach used in choosing the fitting function. That is each term in the peak shape function can

be related to the physics that is taking place during the process of emission of a gamma-ray, its arrival at the detector, and the conversion of a part or all of its energy into an electronic pulse height for analysis. The peak shape plus background is represented by the following terms: (a) For an ideal detector a gamma-ray with a negligible natural width would start out as a sharp line and be broadened by statistical fluctuations in the charge creation process and electronic noise into a Gaussian shape.

$$\Gamma \exp \{- (x/\delta)^2\}$$

where Γ = Amplitude

δ = Width at position x w.r.t. peak position C.

(b) Incomplete charge collection can remove counts from the sharp peak, producing in an ideal detector an exponentially decaying distribution below the peak.

$$\exp (x/\beta) \quad \text{for } x < 0$$

Folding this with a Gaussian noise term of width γ gives

$$\int_{-\infty}^{0} A\Gamma \exp(\tfrac{t}{\beta}) * \exp \{(t-x)^2/\gamma^2\} \, dt$$

$$= A\Gamma \exp(x/\beta) * \tfrac{1}{2} \operatorname{erfc} (x/\gamma + \gamma/2\beta)$$

where A = amplitude of exponential relative to Γ.

erfc (u) = complimentary error function.

(c) For very strong peaks one can observe a much longer exponential tail below the peak, due perhaps to surface effects. Folding this with

a Gaussian noise term gives:

$$T\Gamma \exp(x/\nu) *\tfrac{1}{2} \operatorname{erfc}.\ (x/\mu + \mu/2\nu)$$

(d) Multiple Compton events can produce a step in the background (see S.N.A. method). Also for lower energy gamma-rays, Compton scattering into the detector from surrounding materials can produce a significant step below the peak. A step of amplitude $S\Gamma$, folded with a Gaussian noise term of width σ gives:

$$S\Gamma *\tfrac{1}{2} \operatorname{erfc}\ (x/\sigma)$$

(e) The background B(J) is represented by a first or second order polynomial.

$$B(J) = a + bJ + cJ^2$$

It should be noted that the Gaussian noise width is normally set to be the same throughout (i.e. $\delta = \gamma = \mu = \sigma$). Therefore if there are m peaks in the subregion to be fit, the fitting function for channel J becomes:

$$\begin{aligned} Y(J) = \sum_{I=1}^{m} & \Gamma(I) * \left[\exp(-(x(I,J)/\delta\ (I))^2\right) \\ & + A \exp(x(I,J)/\beta) * \tfrac{1}{2} \operatorname{erfc}\ (x(I,J)/\gamma + \gamma/2\beta) \\ & + T \exp(x(I,J)/\nu) * \tfrac{1}{2} \operatorname{erfc}\ (x(I,J)/\mu + \mu/2\nu) \\ & + S * \tfrac{1}{2} \operatorname{erfc}\ (x(I,J)/\sigma)\Big] + B(J) \end{aligned}$$

Terms (c), (d) and (e) are defined to be part of the continuum.

The N.P.A. is calculated from terms (a) and (b) i.e. N.P.A. = $\Gamma * (\sqrt{\pi} * A * B * \exp(-(0.5 * C/B)^2)$ where $B = \beta/\delta$ and $C = \gamma/\delta$

Minimization is then performed on the function $F(X) = \frac{1}{2} \chi^2$

where $\chi^2 = \frac{1}{ND} \sum_J \left| (K(J) - Y(J))/K(J)^{\frac{1}{2}} \right|^2$

and ND = Number of degrees of freedom.

K(J)= Data at channel J

A final evaluation of the fit is then normally made by studying the χ^2 value. Since this method of evaluation has been shown to be insufficient ([26], it was decided to verify the goodness of fit visually with plots and detailed scans of residuals ([27].

To this end, the calcomp plotting subroutine was modified to be run'interactively' on a high speed graphics terminal, and to allow magnification of any part of the plot.

2.1.4 Test of Analytical Fitting to Doublets

The validity of HYPERMET for evaluating the N.P.A. of doublets was tested using the spectra provided by the I.A.E.A. for their "Intercomparison of Methods for Processing Ge(Li) Gamma-Ray Spectra (G(l))". The purpose of this intercomparison was twofold: (1) to permit each participant to test the validity of his or her own evaluation method. (2) to permit a comparison of different evaluation methods.

Four types of spectrum were provided:

(i) Reference spectrum No. 100. This spectrum contains twenty intense individual peaks. This allows the variation with energy of any peak shape parameters to be determined.

(ii) Spectrum No. 200 contains a number of small photo peaks close to the limit of detection.

(iii) Spectra No. 300-305:- six identical spectra except for differences

due to counting statistics.

(iv) Spectrum No. 400 consists of nine double peaks with various relative intensities and degrees of overlap.

In all spectra No. 200-400, the peak centroids have been shifted and the N.P.A.'s attenuated by known amounts from those in the reference spectrum.

By comparing the shift and attenuation factors measured using HYPERMET to those provided by the I.A.E.A., a measure of the program's ability can be determined.

The results obtained using HYPERMET, for N.P.A. determinations are shown in Table 2.1. It should be noted that it is important to determine the parameters in the peak shape function at various gamma-ray energies from intense peaks (e.g. Spectrum No. 100) first, since in the analysis of most spectra (especially any containing doublets) these shape parameters need to be fixed at known values. (i.e. the data are usually not of sufficient quality to allow them to be determined).

TABLE 2.1 Results for I.A.E.A. Test Spectra

Spectrum number	200	400
True peaks in spectrum	22	18
Peaks detected	17*	18
Spurious peaks	0*	0
error in attenuation factor: $\leqslant 2\sigma$	17	10
$\leqslant 3\sigma$	17	13

* = With some 'fine tuning'of the shape parameters HYPERMET detected

20 true peaks with 5 spurious peaks.

Parr et al ([28] concluded that success in evaluating the test spectra is not so much dependent on the principle of the method used but more on the details of how this method is applied.

2.2.1 Dead-time and Pulse Pile-up Correction

There are two effects which can lead to counting losses in γ-ray spectroscopy: (i) When a multichannel analyser accepts a pulse from a detector, there is a finite time taken to digitize and store the pulse known as dead-time . During this time the multichannel analyser cannot accept any further pulses. (ii) Since the processes of radioactive decay are completely random in time and the resolving time of the electronic system finite, pulses from two events can overlap in time and the two events will sum in amplitude.

The probability of this random summing is proportional to the square of the input pulse rate i.e. Prob (Random sum) α N^2
where N = input pulse rate.

Both the above effects result in a loss of counts from the recorded gamma-ray peak area. For precise intensity measurements, these effects must be corrected for.

Although several techniques exist which correct for deadtime and pile-up ([29-36], the pulser technique as suggested by Anders ([32] and Bolotin et al ([33] is the only method which is capable of a precise correction ([37] and was the method chosen for this work. In the pulser method, a pulser signal of known repetition rate is counted along with all events detected. The area of the pulser peak divided by the number of pulser pulses generated, yields the live-time corrected for pile-up.

$$\text{i.e.} \quad \frac{N_p}{N} = \frac{P_n}{P_o T_c}$$

where N_p = Recorded number of nuclear events

N = Number of events that would have been recorded with zero deadtime and pulse pile-up.

P_n = Recorded number of pulser events.

P_o = Generation rate of pulser signals.

T_c = Real (or Clock) counting time of experiment.

In order to assure the validity of the above relationship, the pulser signals must be introduced into the spectral distribution as if they were a true spectral component of the detected nuclear events. This is accomplished by satisfying three criteria: (1) the shape of the pulser signals entering the preamplifier must resemble that of detector signals, (2) the pulser signals must be introduced into the spectral distribution in random sequence with respect to the pulses of nuclear events, (3) the rate of injected pulser signals must always be maintained at a fixed fraction of the nuclear event rate.

Criterion (1) was satisfied as follows: a gamma source was placed above the detector and pulses from the detector were fed into the preamplifier simultaneously with pulses from the pulse generator. The output pulses from the preamplifier of these two sources were then viewed on an oscilloscope and the rise and fall times of the pulser signals adjusted until the two sets of pulses resembled each other. Unfortunately, a small undershoot on the pulser signals could be observed at the main amplifier output, which would help degrade the shape of the gamma peaks in the recorded spectrum. However, because the pulser frequencies would be much lower than the detector event frequencies, it

was decided that adjusting the pole-zero setting to cater for this undershoot would result in an even greater degradation of peak shape ([38]. The amplitude of the pulser signals is normally set to give the pulser peak at the high energy end of the spectrum where there is a low background ([38].

A block diagram of the pulse-height analysis system used is shown in Fig. 2.2.

The reference pulser output may be triggered in two different modes, each of which ensures the proportionality of the pulser rate to the rate of nuclear events under different experimental conditions. Each output signal of the pulse generator is accompanied by a standard pulser tag that is counted in scaler Number 1., thereby recording the total number of generated pulser signals.

At a constant counting rate, the pulser can be triggered by the internal oscillator (Trigger mode 2). This we will call the Constant Pulser Method (C.P.M.)

When the source rate is decaying the trigger mode is set to position 1. In this position, the fast discriminator continuously monitors the number of pulses arriving from the preamplifier and the output pulses of the discriminator are applied to a fast scaler that resets after a preset number of counted events (= 100). At the end of the scaling cycle, a trigger pulse is output from the scaler and is used to initiate a pulse generator signal that is injected into the preamplifier input. The scaler is reset and a new cycle is started. The pulse generator signal is delayed for an interval long enough ($\geqslant$ 1 msec) to ensure that the multichannel analyser is no longer busy

Fig. 2.2 PULSE HEIGHT ANALYSIS SYSTEM

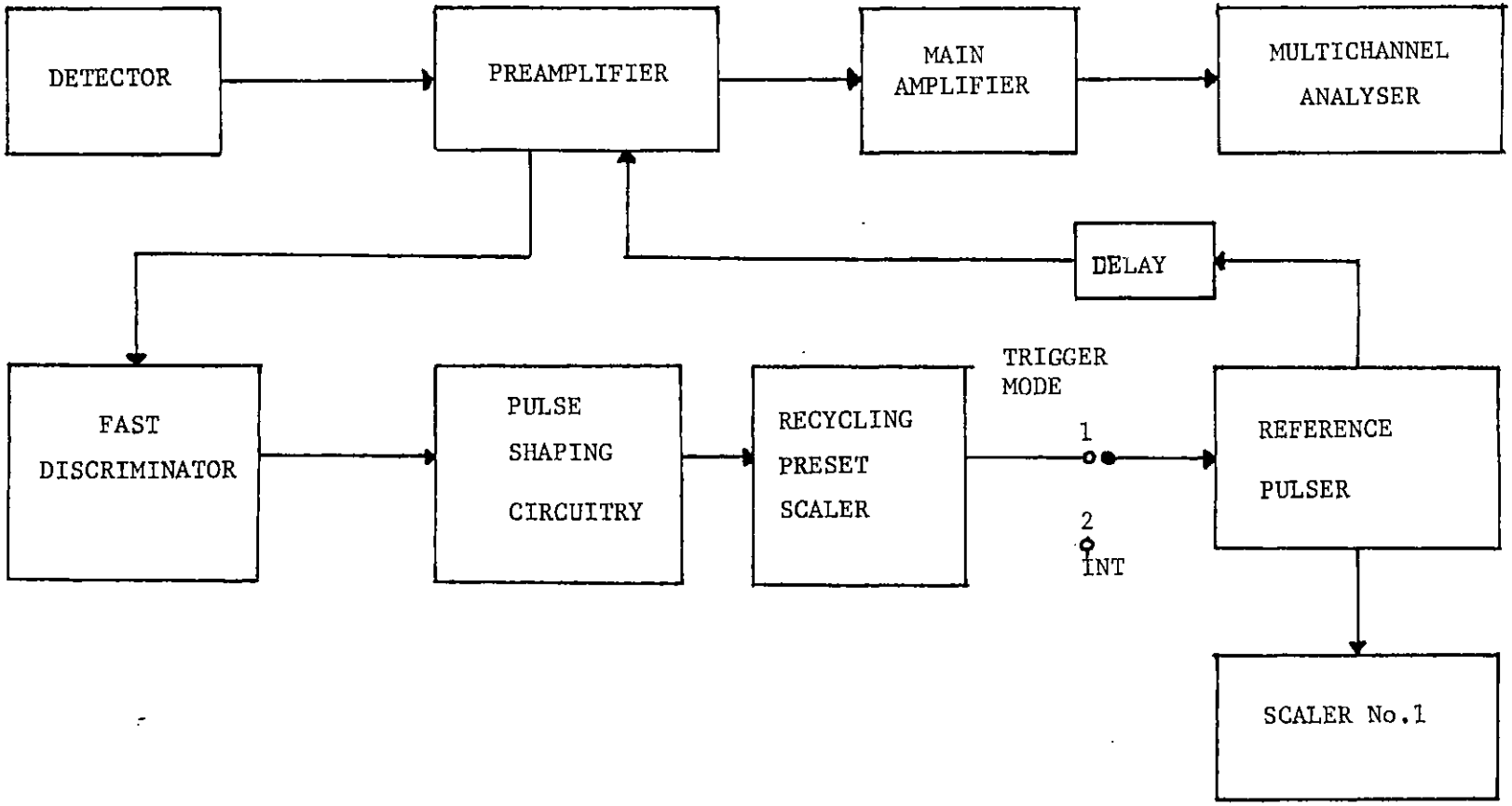

processing the event which initiated the pulser signal. We will call this the Proportional Feedback Method (P.F.M.).

In order to satisfy criterion (3), the duration of each scaling cycle (for the P.F.M.) or the counting period (for the C.P.M.). has to be short compared with the time required for the rate of detected events to undergo a "non-negligible" variation. Because of the uncertainty in the counting losses incurred in the combination of fast discriminator, pulse shaping circuitry and recycling scaler, plus the fact that the P.F.M. only gives more accurate results than the C.P.M. when the counting rate of the detector is time dependent, it was decided to use the C.P.M. whenever possible. According to Junod ([31], the counting rate of a nuclide can be considered independent of time so long as the counting period does not exceed 2% of the nuclide's half-life. In agreement with Wiernik ([39], it has been shown that care has to be exercised when using the C.P.M. otherwise severe systematic errors can be encountered. Wiernik shows that these errors can be avoided if the ratio between the theoretical deadtime produced by the pulser to that produced by the detector signals is kept below 10%.

The pulse generator signal introduced into the spectrum fails the test of true randomness (criterion (2)) in that two consecutive events cannot both be pulser signals (i.e. the pulser cannot sample its own deadtime). Therefore, the pulser events experience lower counting losses than they would have if they were tru ly random. By considering a hypothetical pulser whose output is tru ly random, it can be shown ([33] that the number of observed counts in the pulser peak P_n will be too high by a fraction $\rho\bar{P}_n$

where ρ = deadtime per event (This is a function of channel number)

$\bar{P}_n$ = Average rate of recorded pulser signals = $(\frac{P_n}{T_L})$

The final corrected expression for N is:

$$N = P_o T_c \left(\frac{N_p}{P_n}\right) \left(1 - \frac{\rho P_n}{T_L}\right)^{-1}$$

2.2.2 Errors in Deadtime and Pile-Up Correction

When the rate of detected events is constant, the probability function governing the number of pulser pulses recorded in the analyser follows a binomial (and not a Poisson) distribution. The variance of P_n is then estimated as;

$$\sigma^2_{P_n} = G_o \left(1 - \frac{P_n}{G_o}\right) P_n/G_o$$

$$= P_n \left(1 - \frac{P_n}{G_o}\right) \qquad \text{where } G_o = P_o T_c$$

The variance on N is taken to be:

$$\sigma^2_N \approx N^2 \left\{\left(\frac{\sigma_{P_n}}{P_n}\right)^2 + \left(\frac{\sigma_{N_p}}{N_p}\right)^2\right\}$$

It is assumed that any fluctuations in G_o are negligible.

2.2.3 Test of Deadtime and Pile-Up Correction Method

In order to test the validity of the deadtime and pile-up corrections (and also the N.P.A. determinations) a set of sources provided by the I.A.E.A. for their "Intercomparison of High Precision Gamma-Ray Spectrometry (G-2)", were measured and the results compared with their theoretical values.

The object of the intercomparison was to test the validity of methods for deadtime and pile-up corrections. An ideal measurement method would give results independent of changes in the count rate, peak shape and height of the underlying continuum. Five sources each containing; ^{57}Co, ^{133}Ba, ^{54}Mn and ^{65}Zn were distributed to each of the participants. The count rates of the sources relative to source 1 were about 1 : 3 : 6 : 10 : 15. Each participant had to measure the peak

areas of the four gamma-rays at 112 keV (^{57}Co), 356 keV (^{133}Ba), 834 keV (^{54}Mn) and 1116 keV (^{65}Zn) and report the ratios of the emission rates of source number i to the emission rates of source number 1.

Source preparation:- For each nuclide, the I.A.E.A. determined the activity of the 'stock' solution by measurement in a calibrated 4π-γ ionization chamber. For each of the four stock solutions, weighed quantities were dispensed to 5 solutions (Mix 1, - Mix 5) which were diluted to the intensity ratios 1 : 3 : 6 : 10 : 15. The sources were prepared by depositing weighed amounts of the diluted mix-solutions on to polystyrene discs which were then sealed. Therefore, knowing the values of the specific activities (A_s), the dilution factors for each nuclide (d) and the mass of each source (m), the I.A.E.A. could calculate the activity (A) of a nuclide in a source by:

$$A = A_s \cdot d \cdot m$$

A report of the results of the 91 laboratories which participated in the intercomparison was published in November 1980 ([40]).

The results obtained in this work are shown along with the five best results actually entered for the intercomparison in Table 2.2.

The results are based on the following calculations:

$$C_{ik} = \frac{N_{ik}}{m_i \cdot d_{ik}}$$

where index i = 1,...5 ≡ number of source

k = 1,...4 ≡ number of each nuclide

N_{ik} = peak count rate

M_i = mass of source

d_{ik} = dilution factor

$$\bar{C}_k = \frac{1}{5} \sum_{i=1}^{i=5} C_{ik}$$

$$\Delta_{ik} = 100. \quad \frac{C_{ik} - \bar{C}_k}{\bar{C}_k} \qquad \text{(abscissa used in Fig. 2.3)}$$

$$\delta_k = \frac{1}{5} \sum_{i=1}^{i=5} | \Delta_{ik} | \equiv \text{"DELTA"}$$

$$\bar{\delta} = \tfrac{1}{4} \sum_{k=1}^{k=4} \delta_k \equiv \text{quality parameter used for sorting data}$$

(≡ "Average Delta")

$$R_k = \frac{C_{5k}}{C_{1k}} \equiv \text{"Ratio"}$$

$$\bar{R} = \tfrac{1}{4} \sum_{k=1}^{k=4} R_k \equiv \text{"Average Ratio"}$$

The best results should have $\bar{\delta}$ as small as possible with $\bar{R} = 1$.

As can be seen from Table 2.2 and Fig. 2.3 the measurement and analysis techniques employed in this work provided results comparable with the overall best results submitted for the intercomparison.

2.3.1 Coincidence Summing Corrections

It has been pointed out ([41-44] that for radionuclides emitting two or more cascading photons within the resolving time of the detector, coincident summing will affect the areas of the observed peaks. The magnitude of the effect depends on the specific features of the decay scheme and the solid angle subtended by the detector from the source, but not on the counting rate.

TABLE 2.2 Results for data sorted by average delta value

LAB CODE	AVERAGE DELTA $\bar{\delta}$	AVERAGE RATIO $\bar{R}$	Co - 57		Ba - 133		Mn - 54		Zn - 65	
			DELTA	RATIO	DELTA	RATIO	DELTA	RATIO	DELTA	RATIO
210	0.142	1.004	0.178	1.004	0.156	1.004	0.139	1.005	0.095	1.003
223	0.152	1.001	0.160	0.999	0.113	1.002	0.162	1.003	0.173	1.002
2712	0.187	0.999	0.131	0.996	0.164	0.999	0.277	0.999	0.175	1.000
2612	0.216	1.005	0.129	0.995	0.210	1.006	0.421	1.015	0.103	1.003
241	0.228	0.999	0.320	0.987	0.096	1.001	0.243	1.003	0.251	1.005
THIS WORK	0.143	1.002	0.207	1.003	0.113	1.000	0.142	1.004	0.108	1.000

Fig. 2.3 Results of I.A.E.A. "G-2" Intercomparison

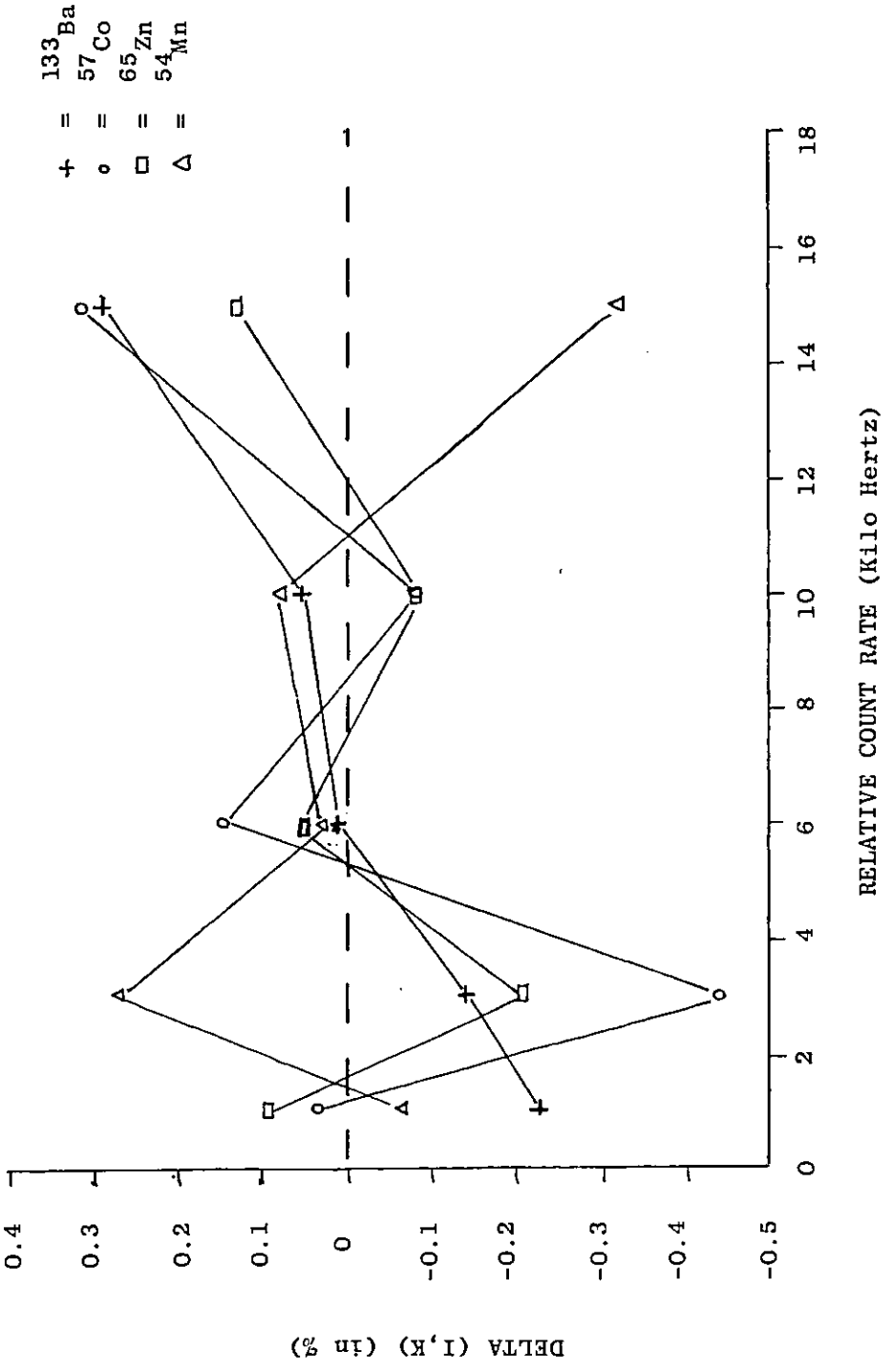

Figure 2.4 A Simple β^- decay scheme

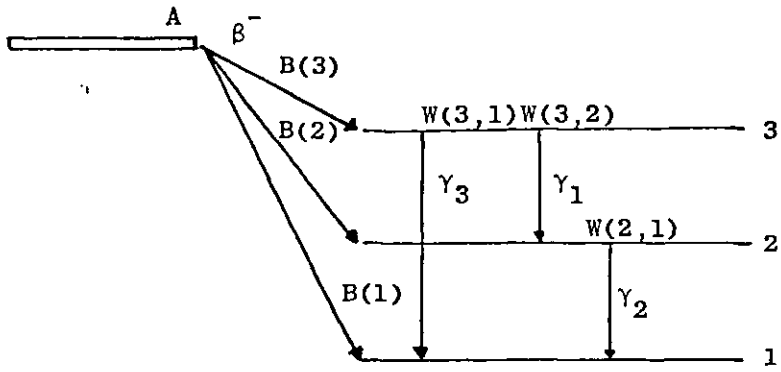

where A = Activity in disintegrations sec^{-1}.

B(I)= Percentage of direct decays to level I sec^{-1}.

W(J,K)= Total branching ratio for transitions from level J to level K

and let α(J,K)= Internal conversion coefficient for transitions from level J to level K

(≡ ratio of the number of internal conversion electrons to the number of gamma quanta emitted).

Ω_K = Fluorescence efficiency

α_K = K-conversion coefficient

ε_p(J,K)= Photo-peak detection probability for the γ-transition from level J to level K

ε_T(J,K)= Total γ-detection probability

ε_T(K) = Total X-ray detection probability

Assuming that any angular correlations between gamma-rays can be ignored, then for the simple decay scheme shown in Fig. 2.4 the rate of pulses recorded in the full energy peak (i.e. photopeak) of gamma-ray γ_2 is given by the following expressions:

(a) Neglecting coincidence summing:

$$\text{Number of } \gamma_2\text{'s in photopeak} = AB(2)W(2,1)\frac{1}{1+\alpha(2,1)}\varepsilon_p(2,1)F(1) + AB(3)W(3,2)W(2,1)\frac{1}{1+\alpha(2,1)}\varepsilon_p(2,1)$$

$$\therefore \quad F(1) = A \quad W(2,1)\ \frac{1}{1+\alpha(2,1)}\ \varepsilon_p(2,1)\{B(2)+B(3)W(3,2)\} \qquad -(2.1)$$

(b) Including Coincidence Summing:

Number of γ_2's in photopeak = A $W(2,1)\ \frac{1}{1+\alpha(2,1)}\ \varepsilon_p(2,1)\{B(2)+B(3)W(3,2)\}$

$S(1)$

$$- AB(3)W(3,2)\ \frac{1}{1+\alpha(3,2)}\ \varepsilon_T(3,2)W(2,1)\ \frac{1}{1+\alpha(2,1)}\ \varepsilon_p(2,1)$$

$$- AB(3)W(3,2)\ \frac{\alpha_K}{1+\alpha(3,2)}\ \Omega_K\varepsilon_T(K)\ W(2,1)\ \frac{1}{1+\alpha(2,1)}\ \varepsilon_p(2,1) \qquad -(2.2)$$

Note: $\frac{\alpha_K}{1+\alpha(3,2)}\ \Omega_K\varepsilon_T(K)$ $\equiv$ prob. of internal conversion from K-shell * prob. x-ray is emitted * prob of detecting x-ray.

Therefore, the correction factor to be applied to the N.P.A. of γ_2 is: $C_1 = eq^n(2.1) \div eq^n(2.2) = F(1)/S(1)$

Similar expressions can be obtained for the correction factors for gamma-rays γ_1 and γ_3 except that the observed rate for γ_3 will be greater than the 'true' rate (i.e. the rate that would be observed in the absence of cascade gamma-rays) due to gamma-rays γ_1 and γ_2 being detected simultaneously.

Note, if we are dealing with an electron capture (E.C.) decay scheme and B(I) represents the percentage of E.C. decays to level I sec^{-1}, then each B(I) in eq^n 2.2 is multiplied by $(1- \varepsilon_T(X)*PK(I)*\Omega_K)$.

where PK(I) = prob. of E.C. from K-shell

Ω_K = prob. of K x-ray emitted in preference to an Auger electron

From the above, it is evident that in order to determine the 'true' detection rate, correction factors must be applied. Although several programs are available which calculate correction factors ([41-43], it

was decided to use the program KORSUM ([43] for this work on the basis that it is the only one which allows for coincident summing of γ-rays with x-rays following internal conversion or electron capture.

KORSUM requires the following input data:

(i) Details of the decay scheme (e.g. type of decay, emission probabilities, fluorescence yields, etc).

(ii) At each source-to-detector distance to be used a set of values for photopeak and total efficiencies for up to 30 energy points. From these values, efficiency curves are set up from which ε_p and ε_T can be calculated for any gamma-ray energy.

The fitting procedure for efficiency curves in KORSUM was modified. The parabolic fit for ln (efficiency) vs ln(energy) was exchanged for a more accurate efficiency function (see Section on efficiency curves).

From this data the program can calculate the correction factor for any gamma-ray of interest, at the relevant source-to-detector distance.

In order to determine the photopeak and total efficiencies needed for the program, it was necessary to take a set of measurements using "single-line" standard sources, for which either no or negligible coincidence summing occurs. The sources used for this were: ^{241}Am (59.5 keV), ^{109}Cd (88.0 keV), ^{57}Co (122.0 and 136.4 keV), ^{139}Ce (165.8 keV), ^{203}Hg (279.1 keV), ^{113}Sn (391.6 keV), ^{85}Sr (513.9 keV), ^{137}Cs (661.6 keV), ^{54}Mn (834.8 keV), ^{65}Zn (1115.4 keV).

Note, if the detector is calibrated with an equally sized standard source of the nuclide under study or if the source-to-detector distance

is large (> 20 cm), then the coincidence summing effects need not be considered.

2.3.2 Errors on Coincidence Summing Corrections

Neglecting any angular correlations between gamma-rays has a negligible effect on the correction factor since as a rule, when the sum effects are observable, the source-to-detector distance is so small that the solid angle correction leads to a rather close approximation : $\bar{W}(0^{o}) = 1$.

From Debertin's ([43] paper, the simplified correction factors (i.e. neglecting any summing with x-rays) for the gamma-rays γ_1, γ_2 and γ_3 shown in Fig. 2.4 are given by:-

$$C_1 = (1-\varepsilon_{T_2})^{-1} \; ; \; C_2 = (1-\left(\frac{P_1}{P_2}\right)\varepsilon_{T_1})^{-1} \; ; \; C_3 = (1+\left(\frac{P_1}{P_3}\right)\frac{\varepsilon_1\varepsilon_2}{\varepsilon_3})^{-1}$$

where P_1 = emission probability of gamma-ray γ_1

ε_1 = photopeak efficiency of gamma-ray γ_1

ε_{T_1} = total efficiency of gamma-ray γ_1

As can be seen, all the correction factors are of the form $(1-x_i)^{-1}$. The error in each correction factor has therefore been assumed to be of the form;

$$(\sigma_{C_i})^2 = \left(\frac{dC_i}{dx_i}\right)^2 (\sigma_{x_i})^2$$

The main sources of error in C_i come from the uncertainties in the total and photopeak efficiencies and if the correction factors are to be calculated with an accuracy of a few percent, the total efficiencies

have to be determined to within an accuracy of about 10%.

2.4.1 Gamma-ray Efficiency Curves

In order to make precise measurements of gamma-ray emission rates it is necessary to accurately determine a calibration of the full energy peak efficiency of the spectrometer system as a function of the γ-ray energy. The most accurate efficiency calibration is obtained experimentally by means of "primary" gamma-ray reference sources, prepared from various radionuclides with γ-rays of different energies and well known emission probabilities. A "primary" reference source is one whose activity has been determined fundamentally by some sort of accurate absolute measurement,([45] (e.g. $4\pi\beta$-γ coincidence counting). A set of such "primary" radionuclides is listed at the end of Section 2.3.1. Since the number of energies at which single γ-ray emitting sources are available is very limited, it is permissible to use other calibration sources such as ^{60}Co, ^{133}Ba and ^{152}Eu to fill in the sparse regions and extend the calibrations to higher energies as long as their γ-ray peak area values are corrected for any coincidence summing effects.

The full energy peak efficiency (or photopeak efficiency) is determined according to the relationship:

$$\varepsilon_p = \frac{N_{corr}}{A_o \cdot D \cdot C}$$

$$\text{with} \quad (\sigma_{\varepsilon_p})^2 = (\varepsilon_p)^2 \cdot \left\{ \left(\frac{\sigma_{N_{corr}}}{N_{corr}}\right)^2 + \left(\frac{\sigma_{A_o}}{A_o}\right)^2 + \left(\frac{\sigma_D}{D}\right)^2 + \left(\frac{\sigma_C}{C}\right)^2 \right\}$$

where ε_p = Full energy peak efficiency

N_{corr} = N.P.A. under photopeak corrected for deadtime, pile-up and coincidence summing.

A_o = Absolute activity in γ's/4π/sec at some reference time.

D = Correction factor for the decay of the standard source between its reference time and the time of counting

C = Correction factor for the decay of the standard source during the counting period.

and $D = \exp(-\lambda t_d)$ λ = decay constant

t_d = time of decay

$C = \{1-\exp(-\lambda t_c)\} / \lambda$ (t_c = counting (or clock) time)

$$\left(\frac{\sigma_C}{C}\right)^2 = \left(\frac{\sigma_\lambda}{\lambda}\right)^2 + \left[\frac{t_c e^{-\lambda t_c}}{(1-e^{-\lambda t_c})}\right]^2 \sigma_\lambda^2$$

$$\left(\frac{\sigma_D}{D}\right)^2 = t_d^2 \sigma_\lambda^2$$

Assuming any errors in t_c and t_d are negligible

It must be noted that when using standard calibration sources produced by different laboratories, for certain radionuclides differences in efficiency values at a single energy of up to 2% can be expected.([46]

It is also important when using different types of standard sources to ensure that the centre of each source is at exactly the same source-to detector distance.

This is because at small source-to-detector distances, significant differences in efficiency can be obtained for very slight changes in the source-to-detector distance.

In general, when measuring γ-ray emission rates, the γ-rays of

interest are at energies different from those used in calibrating the detector, and it is important that an accurate method for interpolating between the measured efficiency values is chosen.

To this end, many semi-empirical analytical functions have been proposed to fit a smooth, continuous curve to the measured efficiency data. The fitting procedure usually being carried out using some sort of least-squares estimation or maximum likelihood method.

Ahmad ([47]) has shown however, that most of these fitting functions are: (a) non-linear in the parameters (which may lead to a bias in the estimate of any interpolated points and their errors) and (b) are usually only able to give a good fit to a limited number of efficiency data sets.

As a result of his survey, Ahmad has proposed the following class of fitting function:

$$\varepsilon(E) = \{P_1 + P_2 \ln E + P_3(\ln E)^2 + P_4(\ln E)^3 + P_5(\ln E)^5 + P_6(\ln E)^7\}/E \qquad - (2.3)$$

which is linear in the parameters and has given satisfactory fits to several sets of efficiency data obtained from different laboratories.

The last term in equation 2.3 is only required if the energy range is to be extended below 120 keV or above 1836 keV. With carefully measured efficiency data, equation 2.3 allows interpolated efficiencies to be determined with a precision of around 1%.

Equation 2.3 was used to fit the efficiency data used in this work and an example of the fit obtained using this function is shown in Fig. 2.5. For coincidence summing corrections, it is also necessary

Fig. 2.5 Photopeak Efficiency for "5 cm" Position on Germanium Detector at N.P.L.

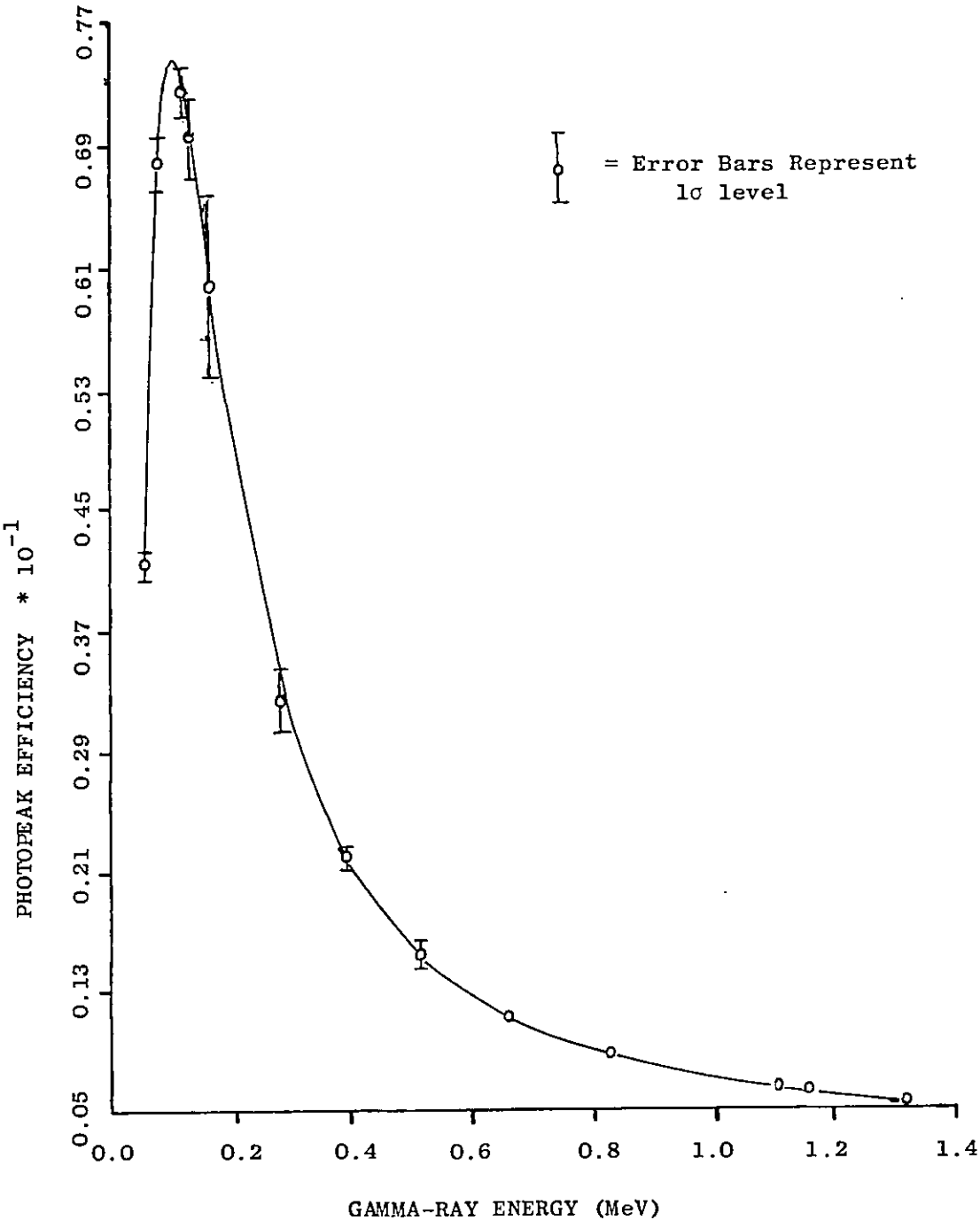

to measure the total efficiency of the spectrometer system. This is done by initially summing all the counts in the spectrum and then (a) removing the contribution from x-rays and other γ-rays by subtraction of known lower-energy contributions or extrapolation of the spectrum through low-energy peak regions, (b) subtracting off the natural background contribution and (c) correcting the residual spectrum for deadtime effects.

The errors in the total efficiency measured this way vary between 2% and 6%,and are mainly due to the subtraction of any low-energy x- or γ-ray contributions. Fortunately, equation 2.3 seems flexible enough to be able to fit total efficiencies as well as photopeak efficiencies and can be used for interpolation between the measured values.

CHAPTER THREE

NEUTRON SELF-SHIELDING

The interpretation of neutron fluence measurements in which the activation method is used must include some assessment of the effects of strong resonances occurring in some of the materials used as detectors.

In particular, whilst the use of a small sample (e.g. a thin foil) generally causes a negligible perturbation in the neutron flux within the medium surrounding the sample, the flux may be greatly depressed in the sample itself due to shielding by its outer regions. This will occur mainly at neutron resonance energies, when the collision mean-free-path in the sample may become comparable to, or small compared with, the sample dimensions. An evaluation of this self-shielding effect is then necessary for the correct interpretation of activation measurements.

The self-shielding factor, G, for a detector is defined as the ratio of the experimental activation to the theoretically expected activation without self-shielding. Defined in this way, the self-shielding factors are always less than unity.

It has been found convenient to split G into two parts: a thermal self-shielding factor for neutrons with energies up to μkT and a resonance self-shielding factor for epithermal neutrons.

Resonance Self-Shielding Factors

These factors have already been studied by several authors ([49-59, 63]; notably G.M. Roe ([49]) for predominantly capture resonances and W.N. Selander

([50]for resonances with appreciable scattering components.

For some materials used in this work however, the literature does not contain any values (e.g. ^{23}Na) or only values with very high uncertainties (e.g. ^{65}Cu). Even for the materials where literature values were available, it was not always evident what the quoted self-shielding factor should multiply (i.e. either a resonance integral or a reduced resonance integral).

For these reasons it was decided to perform a Monte-Carlo type calculation for the self-shielding factors, and to compare where possible, the calculated values with the literature values. The need for such a detailed study of self-shielding factors has also been recently pointed out by Zijp (1982) ([66].

3.1 Monte-Carlo Calculations of Resonance Self-Shielding Factors

In the calculation of the resonance self-shielding factors, the following basic assumptions were made:

a) The neutron flux in the medium surrounding the sample is unaffected by the presence of the sample. This is a good approximation when the sample is placed in a cavity of very large volume compared with the sample volume.

b) The angular distribution of the neutron flux in the medium surrounding the sample is either isotropic or linearly anisotropic, and independent of position, and the energy spectrum of the neutron flux is a known function ($\propto 1/E^{1+\alpha}$)

c) Only s-wave scattering is considered so that scattering is isotropic in the centre-of-mass system (i.e. from quantum-mechanics arguments $kR<<1$, where k = neutron wave vector and R = nuclear radius)

d) Any resonances in the cross-section are assumed isolated from each other so that the Breit-Wigner formula can be used for the cross-section of each resonance.

e) The thickness of the sample is much less than its diameter so that any 'edge-effects' can be neglected.

f) The Doppler effect can be neglected, i.e. The Doppler width given by $\Delta = 2(E_r kT/A)^{\frac{1}{2}}$ is small compared with the total peak width Γ; or that for resonances in which the Doppler effect appreciably broadens the resonance, the self-shielding factors can be corrected in a semi-empirical manor using the results of Roe ([49]

Cross-Sections used in the Monte-Carlo Code

a) Capture cross-section : $\sigma_\gamma(E)$ consider energy ranges as in Fig. 3.1.

Fig. 3.1

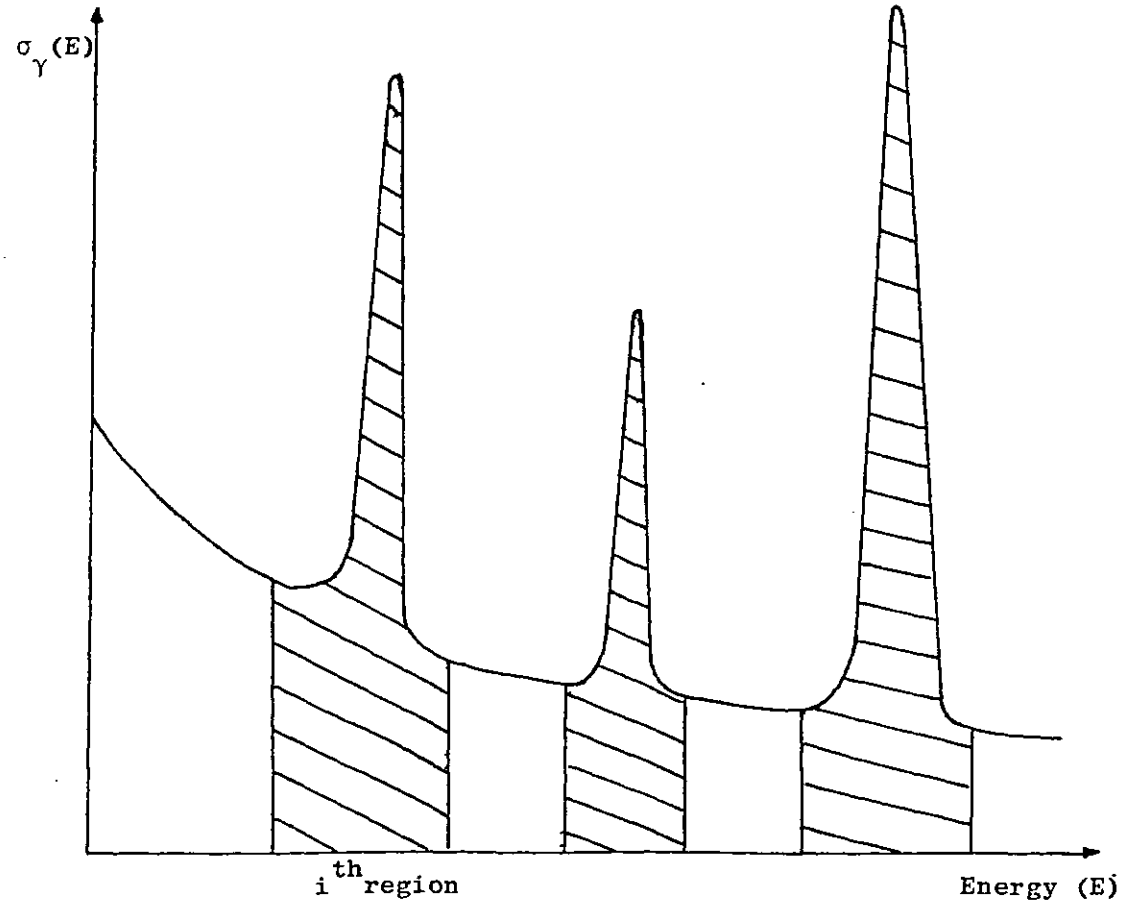

The energy range was divided into resonance-regions (shaded) and those

in which the cross-section is assumed proportional to 1/v (unshaded).

According to assumption (d) there is only one resonance in each shaded area.

In general, for each resonance-region , the cross-section is made up from a Breit-Wigner contribution and a 1/v contribution from all higher energy or unknown resonances.

The total 1/v part of the resonance region is given by $\sigma_{1/v}(E) = \sigma_o \left(\frac{E_o}{E}\right)^{\frac{1}{2}}$ (provided E_o is not in the resonance region) and the general cross-section in this region is given by:

$$\sigma_\gamma(E) = \pi\lambda\!\!\!^{-2}_r \, g\left(\frac{E_r}{E}\right)^{\frac{1}{2}} \frac{\Gamma_n \Gamma_\gamma}{(E-E_r)^2+\frac{\Gamma^2}{4}} + \sigma_o \left(\frac{E_o}{E}\right)^{\frac{1}{2}} \qquad - 3.1$$

Where the first term in equation 3.1 is the Breit-Wigner formula for a single resonance.

and the second term is the sum of the asymptotic forms of the Breit-Wigner formula for all higher energy resonances.

b) Scattering cross-section: $\sigma_s(E)$

The scattering cross-section is made up from two parts, one due to elastic scattering and the other due to inelastic scattering.

Inelastic scattering can only take place when the total kinetic energy of the target atom and the neutron is equal to or greater than the minimum excitation energy of the nucleus. For elements of moderate to high mass number, the minimum excitation energy is usually from 0.1 to 1 MeV. Since none of the resonances considered in this work have energies in this range, inelastic scattering has not been taken into account. The scattering cross-section is then given by:

$$\sigma_s(E) = \frac{\pi\lambda\!\!\!^{-2} g\left(\Gamma_n^2 + \frac{4\Gamma_n R}{\lambda\!\!\!^{-}_r}(E-E_r)\right)}{(E-E_r)^2 + \left(\Gamma/2\right)^2} + 4\pi R^2 \qquad - 3.2$$

where i) the first term represents the compound elastic scattering

ii) the second term arises as the result of interference between neutron waves emitted in compound elastic scattering and potential scattering.

iii) the third term represents the potential or "hard sphere" scattering.

Equation 3.2 is only true for s-wave scattering.

c) Total cross-section : $\sigma_{TOT}(E)$

It was assumed that the value for the total cross-section is given by $\sigma_{TOT}(E) = \sigma_\gamma(E) + \sigma_s(E)$.

The Monte-Carlo program requires as input: the resonance parameters, the "resonance-region" boundaries E_{LB} and E_{UB}, the type of spectrum (i.e.

value of α in $1/E^{1+\alpha}$), the number of neutron tracks to be simulated and details of the element under investigation (i.e. atomic weight, isotopic abundance, density and foil thickness).

For each neutron, its initial energy (between E_{LB} and E_{UB}) and incident angle with respect to the normal at the foil's surface are selected as follows:

Providing that the distribution functions are continuous and finite, assume that there exists a space in which the distributions are rectangular. Then:

Fig. 3.2

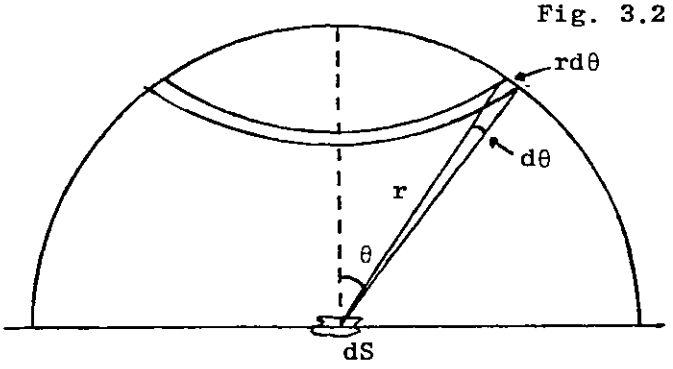

a) For the initial energy E,

$$\gamma = \frac{\int_{E_{LB}}^{E} \phi(E)dE}{\int_{E_{LB}}^{E_{UB}} \phi(E)dE}$$

where γ is a random number in the range $(0 \leqslant \gamma \leqslant 1)$ and $\phi(E)dE$ is the neutron flux in the energy range $E \rightarrow E + dE$ and it is assumed that $\phi(E) = \frac{k}{E}$ is the transformation which makes the distribution rectangular (k = constant). Integrating and rearranging gives:

$$E = E_{LB}\left(\frac{E_{UB}}{E_{LB}}\right)^{\gamma} \qquad -3.3$$

b) For the initial angle, (see Fig. 3.2)

$$\gamma = \frac{\int_{o}^{\theta} 2\pi r \sin\theta r d\theta ds \cos\theta}{\int_{o}^{\pi/2} 2\pi r \sin\theta r d\theta ds \cos\theta}$$

$\gamma = \sin^2\theta = 1-\cos^2\theta$

$\therefore \quad \cos\theta = \sqrt{1-\gamma}$ however, because γ is a random

$\therefore \quad \cos\theta = \sqrt{\gamma}$ number ($0 \leqslant \gamma \leqslant 1$) -3.4

(N.B. For a linear anisotropic flux, $\cos\theta$ is set to 1)

The neutron's path in the foil is then followed until it is either captured in the foil or escapes from it.

In order to determine the type of collision a neutron undergoes whilst in the foil, a sequence of random numbers γ_i (between 0 and 1) is used to find in which of the two intervals they fall.

If $\frac{\Sigma_s}{\Sigma_t} > \gamma_i$ then we have scattering

If $\frac{\Sigma_s}{\Sigma_t} < \gamma_i$ then we have capture

If the neutron undergoes scattering then it is necessary to select its new direction and energy plus the distance travelled to the scattering point.

In particular, it is assumed that the scattering is elastic and isotropic in the centre of mass system and

$$\cos\tilde{\theta} = 2\gamma_i - 1 \; ; \; \chi = 2\pi\gamma_j$$

where $\tilde{\theta}$ and χ are the angles of scattering in the centre of mass system and γ_i, γ_j are independent of each other.

Let μ_{n-1} be the cosine of the angle (w.r.t. the normal to the foil surface) before scattering.

Then after scattering the new direction is given by:

$$\mu_n = \mu_{n-1}\cos\psi + \cos\chi\sqrt{(1-\mu_{n-1}^2)(1-\cos^2\psi)} \qquad -3.5$$

where ψ is the new angle in the lab frame and $\cos\psi = \frac{1+A\cos\tilde{\theta}}{(1+2A\cos\tilde{\theta}+A^2)}$ -3.6

Equation 3.5 is derived as follows (see Fig. 3.3):

Let r be the direction of the neutron after scattering and $\hat{n}$ be a unit vector in the direction of the normal to the foil surface:

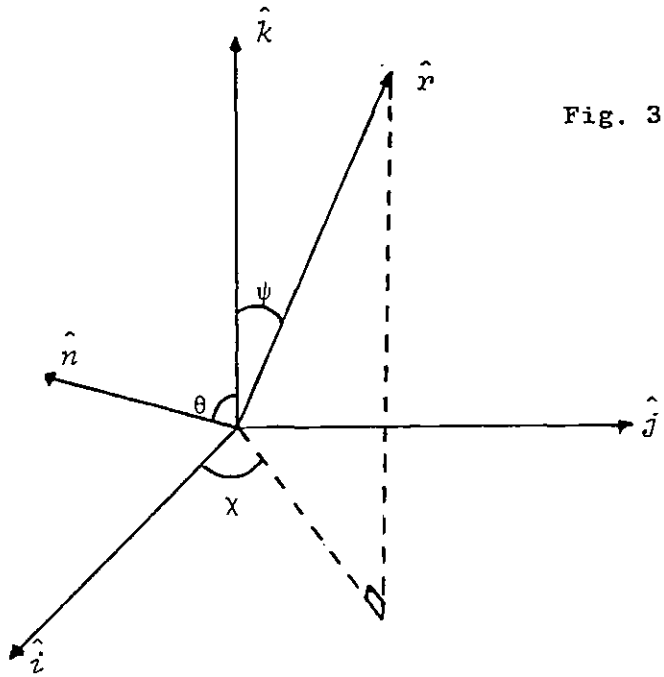

Fig. 3.3.

Then $r = r\hat{r}$

$\hat{r} = \sin\psi\cos\chi\hat{i} + \sin\psi\sin\chi\hat{j} + \cos\psi\hat{k}$

$\hat{n} = \sin\theta\hat{i} + \cos\theta\hat{k}$

Then projection of $\hat{r}$ on $\hat{n}$ is given by $\hat{r}.\hat{n}$ and $\hat{r}.\hat{n} = \cos\theta\cos\psi + \sin\theta\sin\psi\cos\chi$

Since the target atom is assumed to be at rest in the lab frame before the collision, then the new energy of the neutron is given by:

$$E_n = E_{n-1} \frac{(A^2+2A\cos\tilde{\theta} + 1)}{(A+1)^2} \qquad -3.7$$

The distance, X travelled to the scattering point is given by:

$$\gamma = \frac{\int_o^x e^{-\Sigma_t x} \Sigma_t \, dx}{\int_o^{\bar{l}} e^{-\Sigma_t x} \Sigma_t \, dx}$$

$$\therefore X = -\frac{1}{\Sigma_t} \ln (1-\gamma W) \qquad -3.8$$

where W is the probability of a capture or scatter within a distance $\bar{l}$ i.e.

$$W = 1 - \exp(-\Sigma_t(E).t/\cos\theta) \qquad -3.9$$

and t = thickness of foil.

Equations 3.3 - 3.8 agree with those used by Y.A. Schreider ([60].

The program therefore calculates the fraction of neutrons which are captured in the foil and this is equivalent to the experimental activation caused in the foil, by the resonance region under study.

The theoretically expected activation without self-shielding in the same resonance region is calculated as follows:

For no self-shielding,

$$\text{Reactions per neutron} = \frac{\bar{l} \cdot N \cdot \int_{E_{LB}}^{E_{UB}} \sigma_\gamma(E)\phi(E)dE}{\int_{E_{LB}}^{E_{UB}} \phi(E)\,dE} \qquad -3.10$$

where $\bar{l}$ = Mean chord length

N = Target atom density

$\sigma_\gamma(E)$= Absorption cross-section at energy E

$\phi(E)dE$ = Unperturbed neutron flux in interval $E \rightarrow E+dE$

But $\phi(E)dE = \phi_e \frac{dE}{E^{1+\alpha}}$ and ϕ_e is assumed to vary slowly with energy.

The mean chord length, $\bar{l}$ is given by (See Fig. 3.4)

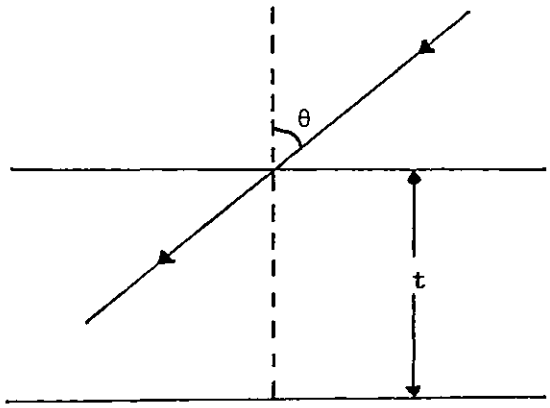

Fig. 3.4.

$$\bar{l} = \frac{\int_0^{\pi/2} 2\pi \sin\theta d\theta \cos\theta \; t/\cos\theta}{\int_0^{\pi/2} 2\pi \sin\theta d\theta \cos\theta} = \frac{\int_0^{\pi/2} t \sin\theta d\theta}{\int_0^{\pi/2} \sin\theta \cos\theta d\theta}$$

$$\bar{l} = \frac{t\left|-\cos\theta\right|_0^{\pi/2}}{\left|\tfrac{1}{2}\sin^2\theta\right|_0^{\pi/2}} = 2t \qquad -3.11$$

$$\text{Reactions per neutron} = \frac{2t\,N \int_{E_{LB}}^{E_{UB}} \frac{\sigma_\gamma(E)}{E^{1+\alpha}} dE}{\int_{E_{LB}}^{E_{UB}} \frac{1}{E^{1+\alpha}} dE} \qquad -3.12$$

But, $\int_{E_{LB}}^{E_{UB}} \frac{\sigma_\gamma(E)}{E^{1+\alpha}} dE \equiv I_{oi}(\alpha)$

where $I_{oi}(\alpha)$ is the effective resonance integral for the resonance-region $E_{LB} \rightarrow E_{UB}$.

$$\text{Number of reactions} = \frac{2n_1 t\ N\ I_{oi}(\alpha)}{\int_{E_{LB}}^{E_{UB}} \frac{1}{E^{1+\alpha}}\, dE} \qquad -3.13$$

where n_1 = number of neutron tracks simulated.

The self-shielding for the resonance region is given by the ratio of the experimental activation to the theoretically expected activation without self-shielding.

In the computation of $I_{oi}(\alpha)$, it has not been assumed that the function $1/E^{1+\alpha}$ may be treated as a constant over the resonance-region.

For $\alpha \neq 0$, both $I_{oi}(\alpha)$ and $\int_{E_{LB}}^{E_{UB}} 1/E^{1+\alpha}\, dE$ are calculated numerically using Simpson's Rule.

3.2 Calculation of Resonance Self-Shielding

From the literature, it can be seen that there are two types of resonance integral which are commonly used;

The normal resonance integral, $I_o = \int_{E_{Cd}}^{\infty} \sigma_\gamma(E) \frac{dE}{E}$ and the reduced resonance integral,

$$I_o' = \int_{E_{Cd}}^{\infty} (\sigma_\gamma(E) - \sigma_{1/v}(E)) \frac{dE}{E}$$

(i.e. the normal resonance integral minus the 1/v contribution)

It seems apparent therefore, that the self-shielding factors needed to premultiply these quantities (the choice depending on the equations being used), will be different for each case.

Consider Fig. 3.1 again.

Case (i): The resonance self-shielding factor for premultiplying a normal resonance integral (assume $\alpha = 0$)

Assume that $I_o = \sum_{i = \text{all shaded regions}} I_{oi} + \sum_{j = \text{all unshaded regions}} I_{oj}$

Define $G_r I_o \equiv \sum_{i = \text{all shaded regions}} G_i I_{oi} + \sum_{j = \text{all unshaded regions}} G_j I_{oj}$

Since in all the unshaded regions, the cross-section varies as 1/v and the self-shielding for 1/v capture is negligible (Selander ([50]), the corresponding self-shielding factors G_j are all very close to unity.

$$\text{Therefore:-} \quad G_r \equiv \frac{\sum_i G_i I_{oi} + \sum I_{oj}}{(\sum_i I_{oi} + \sum_j I_{oj})} \qquad -3.14$$

Equation 3.14 will only be in serious error if there are any important unknown resonances in the cross-section, or if the resonance integral is poorly known.

Case (ii): The resonance self-shielding factor for premultiplying a reduced resonance integral ($\alpha = 0$).

Assuming that the activation in each resonance-region can be theoretically split up into two parts: one due to the resonance part of the cross-section and the other due to the 1/v part.

$$\text{Define} \quad I_{oi} \equiv I'_{oi} + I^{1/v}_{oi}$$

$$\text{and} \quad G'_r \equiv \frac{\sum_{i = \text{all resonance regions}} G_i I'_{oi}}{\sum_{i = \text{all resonance regions}} I'_{oi}} \qquad -3.15$$

In writing equation 3.15 it is assumed that:

$$I_o^{1/v} = \sum_{i = \text{all resonance regions}} I_{oi}^{1/v} + \sum_{j = \text{all non resonance regions}} I_{oj}^{1/v}$$

and $$I_o^{1/v} \approx \sum_i G_i I_{oi}^{1/v} + \sum_j I_{oj}^{1/v} \qquad -3.16$$

Therefore equations 3.14 and 3.15 are consistent with each other unless a significant proportion of the epicadmium 1/v cross-section lies under resonances (in which case equation 3.16 is not valid).

3.3 Comparison of Literature Self-Shielding Factors with those obtained by Monte-Carlo Type Calculations

When comparing values calculated using the Monte-Carlo code with literature values, it was found that it was essential to use the same resonance parameters for the Monte-Carlo calculation as had been used for calculating the literature values. For example, two completely different self-shielding factors were obtained by using the resonance parameters quoted in Selander's work ([50] for Co^{59}, and those quoted in the third edition of BNL-325. (this will be discussed further in the section "Errors involved with Self-Shielding Factors").

Axton ([59] points out that resonance self-shielding factors may be obtained by calculation (e.g. Roe ([49]) or may be derived from cadmium ratio measurements, the latter method in his opinion being considered the more accurate.

Axton's measured self-shielding factors were obtained by measuring the cadmium ratio, R_{Cd} for a very thin foil ($G_{th} = 1$, $G_r' = 1$), solving for $\frac{1}{r}\sqrt{\frac{T}{To}}$ in equation 3.17 (Walker et al. ([62]) and then using the cadmium ratio for a thicker foil to find its self-shielding factor G_r'.

$$R_{Cd} = \frac{\frac{G_{th}}{r}\sqrt{\frac{T}{T_o}} + \frac{G'_r\, s}{g}}{f(\delta)\, G'_r\, (\frac{s}{g} - W) + \frac{1}{K(\delta)}} \qquad -3.17$$

where G'_r = self-shielding factor for resonance neutrons.

$f(\delta)$ = transmission through a cadmium cover of thickness δ, of the resonance neutrons.

G_{th} = self-shielding factor for thermal neutrons.

Note: This equation assumes that the cadmium thickness δ, is sufficient to absorb the thermal neutrons completely,

and $K(\delta) = \frac{1}{4}\sqrt{\frac{\pi E_{Cd}(\delta)}{E_c}}$

Since the self-shielding factors thus measured are valid when premultiplying the quantities $\frac{s}{g}$ and W, which both contain the factor $\int \left[\sigma_\gamma(E) - g\sigma_o(\frac{E_o}{E})^{\frac{1}{2}}\right] \frac{dE}{E}$, they must be of the G'_r type defined above. (i.e. They premulitply a reduced resonance integral).

The experimental self-shielding factors quoted by Jacks ([63] and Baumann ([51] are of a different type from those quoted by Axton.

These authors ([51],[63] obtained their self-shielding factors from the ratio $\frac{(R_{Cd}-1)^o}{(R_{Cd}-1)^x}$ where $(R_{Cd}-1)^o$ refers to an infinitely thin foil and $(R_{Cd}-1)^x$ to a foil of finite thickness.

If one considers a material which obeys the 1/v law below the cadmium cut-off, the epithermal neutron activation between μkT and E_{Cd} can usually be neglected with respect to the activation above E_{Cd} (as long as $\frac{I_o}{g\sigma_o}$ is not very small), and the cadmium ratio is given by equation 3.18.

$$R_{Cd}^{x} = \frac{G_{th}\phi_{th} + G_{r}\phi_{e}\ \{f_2(\alpha) + (\frac{E_1}{E_r})^{\alpha}\ \{\frac{I_o}{g\sigma_o} - f_2(0)\}\}}{G_{r}\phi_{e}\ \{f_2(\alpha) + (\frac{E_1}{E_r})^{\alpha}\ \{\frac{I_o}{g\sigma_o} - f_2(0)\}\}} \qquad -3.18$$

All quantities in equation 3.18 are defined in section on "Flux convention".

However, the quantity $(R_{Cd}-1)^{x}$ is given by

$$(R_{Cd}-1)^{x} = \frac{G_{th}\phi_{th}}{G_{r}\phi_{e}\ \{f_2(\alpha) + (\frac{E_1}{E_r})^{\alpha}\ \{\frac{I_o}{g\sigma_o} - f_2(0)\}\}} \qquad -3.19$$

The quantity $(R_{Cd}-1)^{o}$ is obtained by putting $G_{th} = G_{r} = 1.0$ in equation 3.19.

Therefore, $\frac{(R_{Cd}-1)^{o}}{(R_{Cd}-1)^{x}} = (\frac{G_r}{G_{th}})$

That is, the self-shielding factor obtained in this way premultiplies a normal resonance integral.

The numerical calculations of Roe([49] and Selander ([50] are of the type G_r' and are usually quoted for individual resonances.

In order to test the Monte-Carlo code fully, a comparison between Monte-Carlo values and literature values should be made for the two cases : (a) where the resonances are predominantly capture.
and (b) where the resonances include an appreciable scattering component.

a) Capture resonances.

Comparisons of Axton's and Baumann's results for gold with those obtained from the Monte-Carlo code are given in Table 3.1 and Fig. 3.5. respectively. The Monte-Carlo calculations included the effects of the first three main resonances at 4.9, 60 and 107 eV. The effect of the

Fig. 3.5. A Comparison Between M-C Values and Baumann's Values for Self-Shielding Factors (Including "1/v part") for ^{197}Au

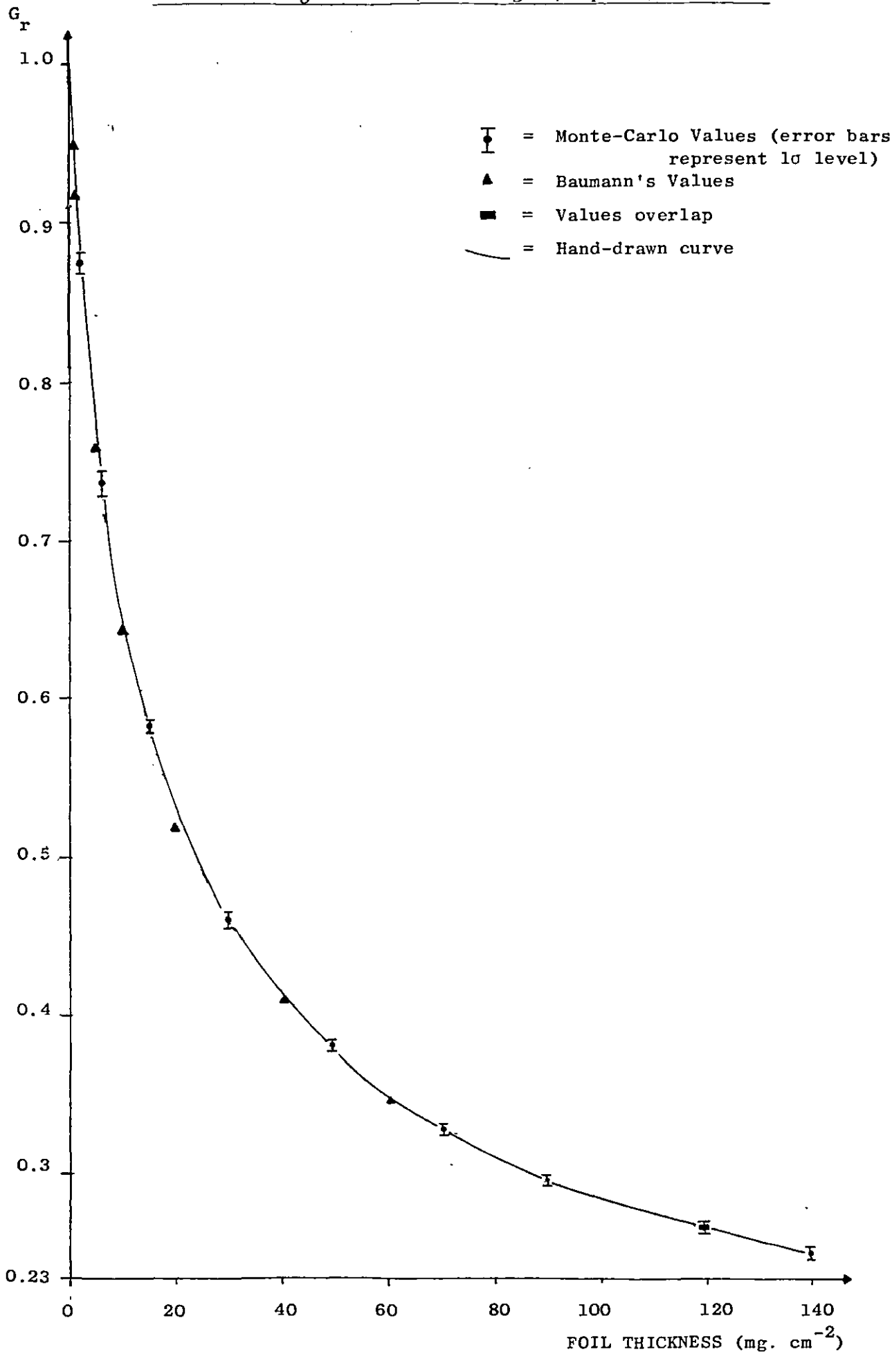

other resonances was small and had a negligible influence on the final self-shielding factor.

It can be seen that in both cases, the agreement is very good.

Table 3.1

Thickness (cm)	Monte-Carlo G_r	Axton G_r
3.105×10^{-4}	0.727 ± .009	0.710
1.552×10^{-3}	0.440 ± .005	0.441
2.277×10^{-3}	0.378 ± .005	0.380

When comparing the Monte-Carlo values for gold with the calculations of Roe, the capture cross-section used in the code was restricted to the first term in equation 3.1.

It was found that although the Monte-Carlo values agreed to within better than 2% of the Roe calculations (at $0^{o}K$), they were consistently higher. This is because the Roe calculations do not take scattering into account which has the effect of increasing the self-shielding factor.

b) Scattering Resonances

The Monte-Carlo values for the resonance self-shielding factor for the 337 eV ^{55}Mn resonance are compared with Selander's calculated values for different foil thicknesses in Table 3.2.

As can be seen from Table 3.2, the agreement between the Monte-Carlo values and Selander's values is good. Similar agreement was obtained for the 1080 eV resonance.

The Monte-Carlo calculations were also compared with Axton's

Table 3.2

Thickness (cm)	Monte-Carlo G_r'' (M)	Selander G_r' (S)	$(\frac{S-M}{S}) \times 100$
6.125×10^{-4}	0.9722 ± 1.7%	0.979	0.69
1.715×10^{-3}	0.9394 ± 1.3%	0.944	0.47
5.145×10^{-3}	0.8621 ± 1.6%	0.862	-0.01
1.016×10^{-2}	0.7722 ± 0.88%	0.778	0.74
1.524×10^{-2}	0.7090 ± 0.87%	0.716	0.94
2.032×10^{-2}	0.6583 ± 0.7%	0.671	1.89

measured values for manganese, in the form of Mn/Ni foils.

Although Axton's values were consistently lower than the Monte-Carlo values, the agreement was still to within 2%. The difference between the Monte-Carlo values and these experimental values may be due to interference effects between the manganese and cadmium resonances.

Fig. 3.6 shows the difference between G_r and G_r' resonance self-shielding factors for ^{55}Mn (calculated using Selander's partial width values). It can be seen that at moderate foil thickness, the discrepancy is of the order of ten percent, thus showing the importance of differentiating between the two cases.

3.4 The Effect of a "Non 1/E" Spectrum in the Calculation of Self-Shielding Factors

The epithermal neutron spectrum can only be theoretically assumed to follow a 1/E law under special conditions:

Fig. 3.6 A Comparison between Calculated G_r and G_r' Self-Shielding Factors for ^{55}Mn

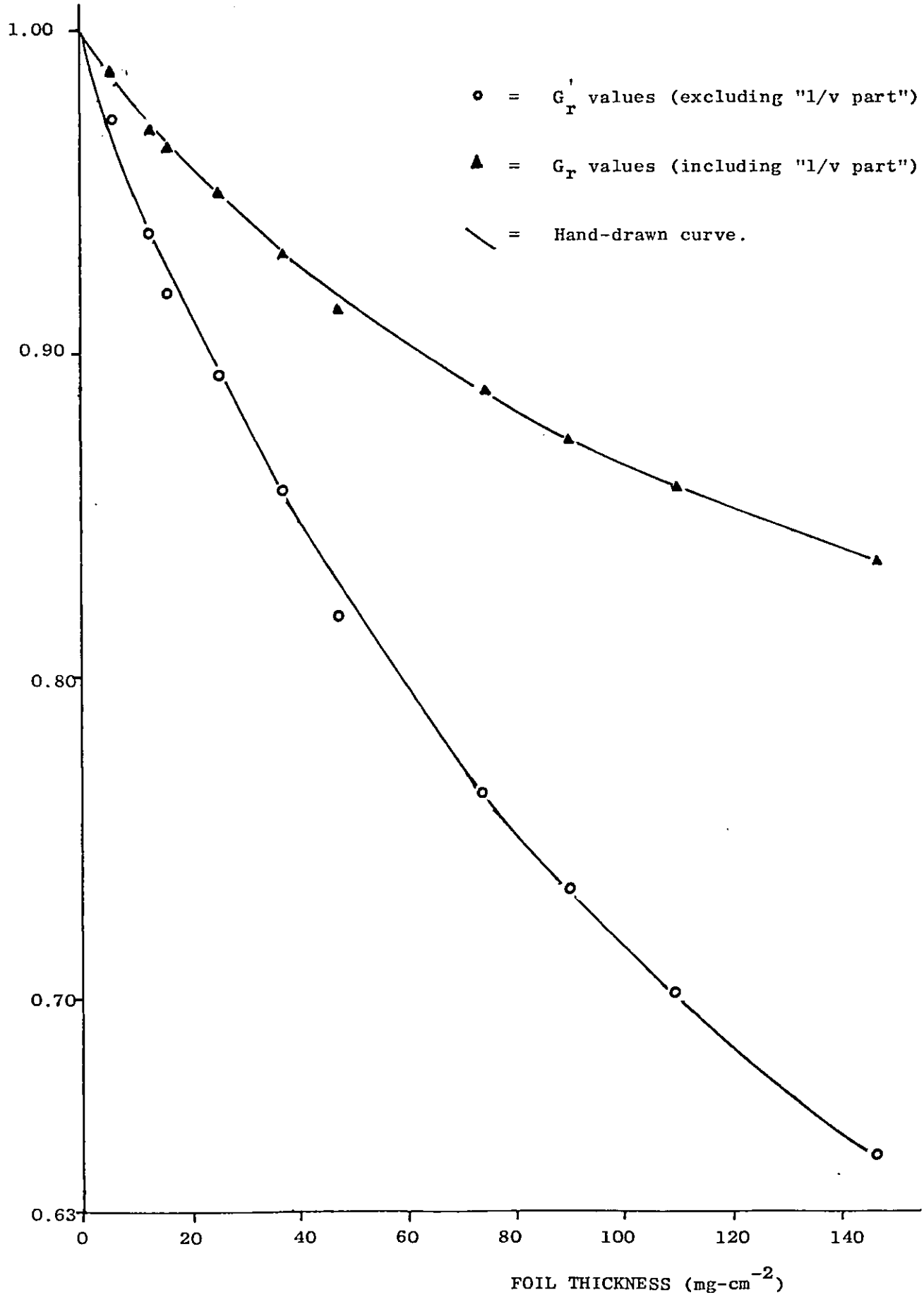

a) The medium in which the fast neutrons are being slowed down is homogeneous and infinite (i.e. no leakage)

b) The fast neutron sources are homogeneously distributed in space.

c) The energy slowing down power $\xi\Sigma_s$, does not depend on energy.

d) During the moderation process there is no absorption.

e) The moderating atoms behave as free particles and have the same mass as a neutron.

These conditions are not satisfied in practice and it has been assumed ([11] that any deviations from a 1/E spectrum can be represented by a variable α in the form of $1/E^{1+\alpha}$.

Since foil detectors are nearly always measured under conditions which do not meet the requirements (a) - (e) above, it is necessary to study the effects of a non -1/E spectrum (i.e.$\alpha \neq 0$) on the calculation of self-shielding factors.

Monte-Carlo calculations were performed for the isotopes ^{197}Au and ^{55}Mn for various spectrum shapes. The resulting G_r' values are shown in Table 3.3.

The gold calculations include the effects of the first three main resonances at 4.9, 60 and 107 eV; the manganese calculations include the 337 and 1098 eV resonances.

The alpha values (α) were selected to cover the range experienced most often practically.

From these results it can be seen that the value of alpha (for $\alpha \leqslant 0.2$) has a negligible effect on the resonance self-shielding factor

Table 3.3 The Variation of G_r' with α for ^{197}Au and ^{55}Mn

Element	α	G_r'	+/-
Gold -197	0	0.3380	0.0011
	0.05	0.3385	0.0012
	0.10	0.3379	0.0014
	0.15	0.3366	0.0010
	0.20	0.3373	0.0011
Manganese -55	0	0.8234	0.0083
	0.05	0.8307	0.0081
	0.10	0.8329	0.0084
	0.15	0.8312	0.0078
	0.20	0.8329	0.0076

even when the total width of the resonance may change by a factor of one hundred or more* (*see nuclear parameters for the main 4.9 eV ^{197}Au and 337 eV ^{55}Mn resonances).

Since in this work the worst case of Doppler broadening of a resonance (i.e. in the 229 eV resonance of ^{65}Cu) increases the "resonance width" by much less than this, it is assumed that the effect of a non -1/E spectrum in the calculation of the self-shielding factor at some temperature $T > 0^{o}K$ (i.e. including Doppler broadening) will also be negligible.

3.5 Errors on Resonance Self-Shielding Factors

On each run, the Monte-Carlo code calculates twenty self-shielding

factors and from these, estimates of the mean value and the standard error on the mean are made using the formulae

$$\text{Mean values, } \bar{x} \equiv \frac{1}{N} \sum_{i=1,N} x_i \qquad -3.20$$

$$\text{Standard error on the mean } \sigma_{\bar{x}} = \frac{\sigma}{\sqrt{N}} \qquad -3.21$$

where σ, the sample standard deviation, is given by

$$\sigma^2 \approx \frac{1}{N-1} \sum_{i=1,N} (x_i - \bar{x})^2$$

and N = number of observations

x_i = value of i^{th} observation.

That is, the errors given by the Monte-Carlo code are only the random errors due to the statistics and do not include any systematic errors.

Types of systematic error which may occur are:

i) Any inconsistencies in the nuclear data used for describing each resonance may lead to a self-shielding factor completely different from the true self-shielding factor at the foil thickness under study. It has been pointed out that in fact many of the width parameters at low energies may be in error.

Incorporating the complex error analysis needed to take any data inconsistencies into consideration into the Monte-Carlo code, would make the code extremely slow and far too expensive to run practically.

It was therefore felt that the best way of taking data incon-

sistencies into account was to first evaluate all the data available carefully, and then to estimate the effect on the self-shielding factor from any possible spread in these best data values (i.e. by running the code at the two extremes of the spread).

ii) Any unknown resonances which may contribute significantly to the resonance integral would lead to a calculated self-shielding factor which would be too high, (i.e. it would suggest that there was less shielding than there actually was).

iii) The resonances are too closely spaced which means that; (a) the Breit-Wigner formula does not accurately represent the shape of each resonance (needing to be replaced by some multi level formula) and (b) there may be interference between neighbouring resonances, since neutrons scattered from the higher energy resonance can be captured in the lower energy resonance, slightly increasing its effective self-shielding factor, and there may be some shielding between resonances which decreases the self-shielding factor.

iv) Correcting for Doppler broadening using Roe's work will not be adequate for samples in which crystalline binding is significant.

v) The shape of the neutron spectrum in which the foil is being irradiated, may not be of the form $1/E^{1+\alpha}$, e.g. consider a foil irradiated under cadmium. If the foil has a resonance in the energy range $(1-\alpha)\ E_r(Cd)$ below a cadmium scattering resonance

where $\alpha = \left|\frac{A-1}{A+1}\right|^2$ A = atomic weight of cadmium

and $E_r(Cd)$ = energy of cadmium scattering resonance,

then the flux seen by the foil will be enhanced in the region of the foil resonance and diminished in the region of the cadmium resonance.

However, due to the good agreement between experimental and calculated self-shielding factors, it is believed that none of the above effects is serious, or at least that they are self cancelling.

3.6 Thermal Self-Shielding Factors

For foils irradiated in a cavity (so that any external flux depression is negligible), thermal self-shielding factors, G_{th} are normally calculated using Maxwellian averaged cross-sections in equation 3.23.

$$G_{th} = \frac{1-2E_3(\tau)}{2\tau} \qquad -3.23$$

where $\tau = N\sigma_{eff}t$ and $E_3(\tau) = \int_1^\infty \frac{e^{-\tau u}}{u^3}\,du$

σ_{eff} = The effective microscopic absorption cross-section per atom.

N = Atom density of foil (i.e. atoms cm^{-3})

t = Thickness of foil.

Equation 3.23 is only strictly true for an isotropic and monoenergetic neutron flux incident on a slab absorber.

There are therefore two main sources of error in using equation 3.23 for calculating G_{th} values:

a) For some of the foils used in this work, the scattering cross-section at thermal energies is of the same order of magnitude as the absorption cross-section.

b) It has been pointed out ([64] that there are problems involved in deciding on the correct cross-section to be used when extending the one-velocity treatment to the case of a Maxwellian velocity

distribution. This choice is critical since when a foil with a 1/v absorption cross-section absorbs an appreciable number of the lower energy neutrons, there will be a spectral shift (hardening) of those neutrons which traverse the foil.

Some authors ([51,65] calculate the effective cross-section to be used according to equation 3.24.

$$\bar{\tau} = \frac{\int_0^\infty \tau(v)\phi(v)dv}{\int_0^\infty \phi(v)dv} \qquad -3.24$$

Since we are dealing with a 1/v detector in a Maxwellian spectrum then

$$\tau(v) \alpha 1/v \; ; \quad \phi(v) \alpha v^3 e^{-v^2/v_o}$$

and $$\bar{\tau} = \frac{\sqrt{\pi}}{2} \tau_o \qquad -3.25$$

(The subscript $_o$ denotes the value at the most probable velocity).

However, it is believed that this is not the correct cross-section to be used when calculating a self-shielding factor, for the following reasons:

From the definition of self-shielding, at each velocity;

$$\frac{A_c(v)}{A_o(v)} = \frac{\alpha(v)}{2\tau(v)}$$

where: $\alpha(v) = 1-2E_3(\tau)$

$A_c(v)$ = Activity of a foil of thickness t

$A_o(v)$ = Activity of an infinitely thin foil

Integrating over all velocities gives:

$$2\int_0^\infty A_c(v)\,\tau\,(v)dv \;=\; \int_0^\infty A_o(v)\,\alpha\,(v)dv$$

or $\quad 2\,A_c\bar{\tau} \;=\; A_o\bar{\alpha}(v)$

$$\text{where}\quad \bar{\tau} \;=\; \frac{\int_0^\infty \tau(v)A_c(v)dv}{\int_0^\infty A_c(v)dv} \qquad -3.26$$

$$\text{and}\quad \bar{\alpha}(v) \;=\; \frac{\int_0^\infty \alpha(v)A_o(v)dv}{\int_0^\infty A_o(v)dv} \qquad -3.27$$

From equation 3.26 it can be seen that the cross-section should be weighted by the activity and not the flux when calculating a self-shielding factor.

Integrating 3.26 gives,

$$\bar{\tau} \;=\; \frac{2}{\sqrt{\pi}}\;\tau_o \qquad -3.28$$

Equation 3.28 is applicable only for the case of a very thin foil, and will reduce as spectral hardening occurs. The use of equation 3.28 for calculating the effective cross-section agrees with the work of Axton ([59] and Ryves ([58].

As far as the scattering problem is concerned, it has been said ([52] that the error introduced by neglecting scattering is only appreciable if the scattering cross-section is much larger than the absorption cross-section. Even so, for sufficiently thin foils, Zweifel ([54] gives a formula which takes into account the effects of internal scattering.

$$G_{th} \;=\; \frac{G^o_{th}}{1 - C_s(1-G^o_{th})} \qquad -3.29$$

where C_s is the ratio of scattering to absorption in the sample.

G^o_{th} is the self-shielding factor calculated with C_s set to zero.

However, because of the problem in selecting a σ_{eff} to be used in equation 3.23, a Monte-Carlo code similar to that used in the calculation of resonance self-shielding factors, was developed to calculate thermal self-shielding factors.

The G_{th} values calculated by the code were then compared with the G_{th} values calculated using equation 3.29.

3.7 Monte-Carlo Calculation of Thermal Self-Shielding factors

The Monte-Carlo code for calculating thermal self-shielding factors is modelled on the code used for resonance self-shielding factors with the following important changes:

a) The capture cross-section is given by:

$$\sigma_\gamma(E) = g\sigma_o \left(\frac{E_o}{E}\right)^{\frac{1}{2}}$$

where g is the Westcott factor accounting for the deviation of the cross-section from the 1/v law in the thermal region.

σ_o is the 2200 ms^{-1} cross-section

E_o is the 2200 ms^{-1} energy

and the scattering cross-section is assumed to be energy independent and given by the potential scattering term, $\sigma_s = 4\pi R^2$

b) In the thermal energy range, the thermal motion of the scattering atoms has to be taken into account. This is done by assuming that the scattering atoms can be considered as a gas with a Maxwellian

distribution of velocities, since the neutrons are assumed to be in thermal equilibrium with the moderating atoms, then the energies of the scattering atoms plus the initial energy of the incoming neutron are selected as follows:

$$\gamma = \frac{\int_0^E P(E)dE}{\int_0^\infty P(E)dE} \qquad -3.30$$

where γ is a random number in the interval $(0 \leqslant \gamma \leqslant 1)$, and the probability distribution $P(E)$ is of the form $P(E) = \text{const. } E\, e^{-E/kT}$

Integrating equation 3.30 gives:

$$\gamma = 1 - e^{-E/kT} \quad (1 + E/kT)$$

which is a transcendental equation of the form

$$\varepsilon = (1 + y)e^{-y} \qquad -3.31$$

where $\varepsilon = 1-\gamma$ and $y = E/kT$ and has to be solved numerically for y, using an iterative method.

Appendix I shows how the scattering angles and the new energy of the neutron after scattering are calculated.

c) The theoretically expected activation without self-shielding is given by

$$\text{Number of Reactions} = n_1 \cdot 2t \cdot g \cdot N \cdot \sigma_o \cdot \frac{\sqrt{\pi}}{2} \qquad -3.32$$

(All the quantities have been defined previously).

A comparison of the values obtained using the Monte-Carlo code with the values obtained using equation 3.29 for ^{197}Au and ^{55}Mn is

shown in Table 3.4.

It can be seen that the best agreement is obtained when a value for the effective cross-section as calculated by equation 3.28 (with an allowance for spectral hardening for ^{197}Au), is used in equation 3.29.

Table 3.4

Element	Foil Thickness ($mg\ cm^{-2}$)	Zweifel (Z) σ_{eff}/σ_0	Zweifel (Z) G_{th}	Monte-Carlo(M) G_{th}	$\left(\frac{M-Z}{M}\right) \times 100$
^{197}Au	20	0.886	0.9849	0.9825	-0.24
		1.05	0.9827	±0.003	-0.02
		1.08	0.9823		-0.02
^{197}Au	297	0.886	0.8625	0.8449	-2.08
		1.05	0.8448	±0.0004	0.01
		1.08	0.8417		0.37
^{55}Mn	37	0.886	0.9876	0.9838	-0.37
		1.05	0.9858	±0.001	-0.19
		1.08	0.9854		-0.15
		1.20	0.9841		-0.02
^{55}Mn	200	0.886	0.9504		-1.93
		1.05	0.9434	0.9324	-1.17
		1.08	0.9421	±0.0010	-1.04
		1.20	0.9372		-0.51

Due to the excellent agreement and the expense of running the Monte-Carlo code, it was decided to calculate the G_{th} values to be used in this work, using the equation of Zweifel. An effective cross-section of $\sigma_{eff} = 1.05\ \sigma_o$ was used since agreement with the Monte-Carlo values for the foil thickness' used in this work was to within 0.5%.

CHAPTER FOUR

RECALIBRATION OF THE N.P.L. THERMAL NEUTRON FLUX FACILITY

The purpose of this experiment was to recalibrate the thermal neutron flux facility at the National Physical Laboratory, Teddington, Middlesex, in terms of the three flux parameters, Φ_{th}, ϕ_e and α which are described in Section 4.2. By use of the (n,γ) reaction, experimental activation data for several isotopes with a wide range of effective resonance energies, were used to determine the above flux parameters for the "2 cm" position in the thermal pile. The values obtained are in good agreement with the values measured by Ryves and Paul in 1968. This chapter contains details of the experiment and describes the use of a least-squares minimization program for estimating the flux parameters and providing information on the input data used for the nuclear data.

4.1 N.P.L. Standard Thermal Neutron Flux Facility

A schematic diagram of this flux facility is shown in Fig. 4.1. Neutrons are produced by using a Van de Graaff accelerator to accelerate deuterons down an evacuated beam line on to two beryllium targets where the stripping reaction $^{9}Be(d,n)^{10}B$ takes place. Only some of the states in ^{10}B are strongly excited by the reaction and neutrons produced in this way are formed in several different energy groups corresponding to these excited states. The number of groups formed depends on the energy of the incoming deuteron beam. The accelerator beam is led down the centre line of the graphite assembly and the semi-circular beryllium targets are placed at 80 cm upstream and 80 cm downstream of the centre of symmetry of the graphite block. The targets are surrounded

Fig. 4.1 A Schematic Drawing of the Thermal Neutron Flux Facility

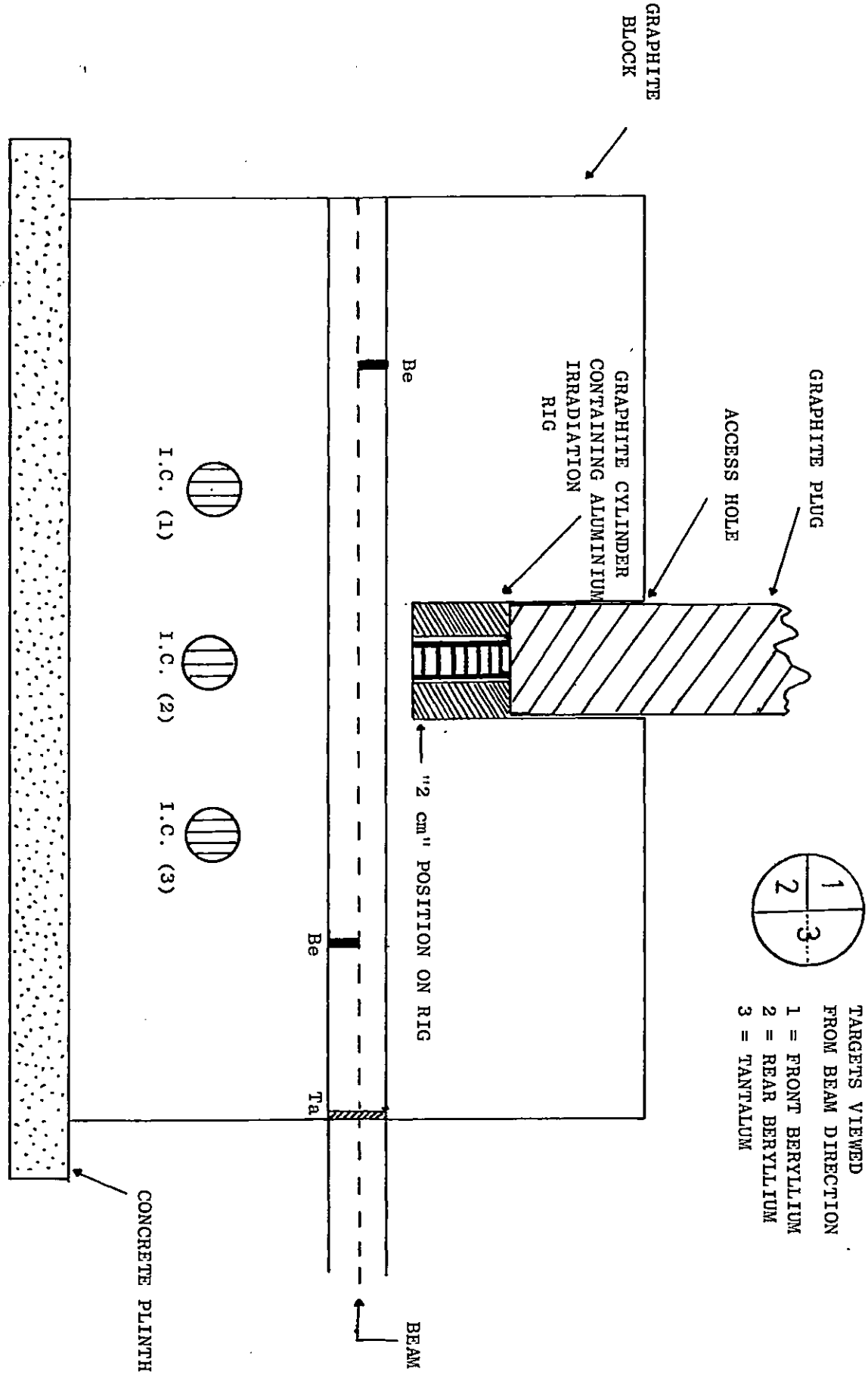

by 2.5 cm of Pb to reduce the γ-ray intensity and immediately behind each target is a 5 cm thick polythene block to moderate the forward directed neutrons. The beam is scanned over the target by means of an oscillating potential applied to the B set of deflector plates (See Fig. 4.2). This is to avoid any damage to the targets. The Flux at the centre of the graphite block is controlled by three boron-coated ion chambers (I.C.(1)...I.C.(3)) placed 20 cm below the beam line and respectively 46 cm upstream, central and 46 cm downstream. The upstream and downstream chambers control the vertical positioning of the beam on the beryllium targets by applying voltage to the vertical A plates. This has the effect of controlling the gradient of the flux between the two ion chambers. The central ion chamber controls the horizontal positioning of the beam so that it is either on the targets or on the tantalum sector which produces no neutrons by applying voltage to the horizontal A plates.

This controls the flux level at the central position and is done by comparing the voltage developed by the ion chamber current across a standard resistor with a chosen reference voltage. The output from the central chamber can also be monitored in the control room enabling corrections to be made for any time variations in the flux level. A fuller description of this facility is given by Ryves ([6].

4.2 Neutron Flux Convention

The neutron flux convention used in this work is taken from Ahmad et al([67] and is reproduced here for the sake of clarity.

The reaction rate, or saturated activity per target atom for an (n,γ) type nuclear reaction is given by:

$$A = \Phi_{th}\,\sigma_{th} + \phi_e I_o(\alpha) \qquad -4.1$$

Fig. 4.2 Side view of the Beam Handling before it enters the Moderator Block, A, B and C are sets of Deflector Plates.

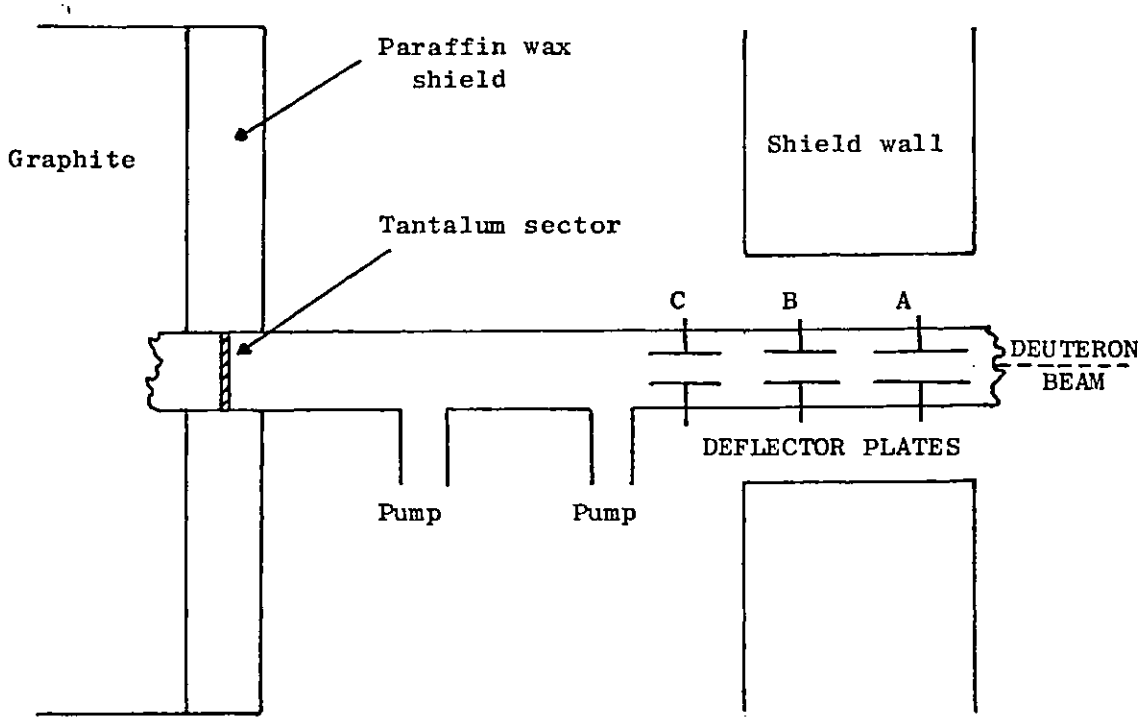

where Φ_{th} is the conventional Maxwellian thermal flux equal to $n_{th}v_o$, the product of the thermal neutron density, and the reference speed of 2200 ms^{-1}.

ϕ_e is the epithermal flux per unit ℓnE at energy E_1, which is an arbitrary energy chosen for convenience to be 1eV.

i.e. $$\phi_e = E_1^{-\alpha} E^{1+\alpha} f_e(E) \quad (E \geq \mu kT) \qquad -4.2.$$

where $f_e(E)$ is the epithermal neutron flux density per unit energy, assumed proportional to $1/E^{1+\alpha}$, and μkT is the energy dividing the thermal region from the epithermal region (μ is usually taken to be 5).

σ_{th} is the effective activation cross-section for cadmium absorbable neutrons.

i.e. $$\sigma_{th} = g\sigma_o + \frac{\phi_e}{\Phi_{th}} \int_{\mu kT}^{E_{Cd}} \sigma(E) \frac{E_1^{\alpha}}{E^{1+\alpha}} dE \qquad -4.3$$

where E_{Cd} is the effective cadmium cut-off energy. $I_o(\alpha)$ is the effective resonance integral, which depends on the value of α:

$$I_o(\alpha) = \int_{E_{Cd}}^{\infty} \sigma(E) \frac{E_1^{\alpha}}{E^{1+\alpha}} dE \qquad -4.4$$

In order to deal with the integral from μkT to E_{Cd} which appears in equation 4.3, introduce the dimensionless quantity $W'(\alpha)$:

$$W'(\alpha) = \frac{1}{\sigma_o} \int_{\mu kT}^{E_{Cd}} \left(\sigma(E) - \frac{g\sigma_o v_o}{v}\right) \frac{E_1^{\alpha}}{E^{1+\alpha}} dE \qquad -4.5$$

The factors g and W' allow for deviations from a 1/v cross-section in the thermal region, and in the region between μkT and E_{Cd} respectively.

For a 1/v cross-section g = 1 and $W' = 0$. According to Ahmad ([11], because the correction is usually small it is nearly always justified in replacing $W'(\alpha)$ with W' (i.e. the case where $\alpha = 0$).

Combining equations 4.1, 4.3 and 4.5 gives:

$$A = \Phi_{th} g\sigma_o + \phi_e \left[\sigma_o W' + g\sigma_o f_1(\alpha) + I_o(\alpha)\right] \qquad -4.6$$

where $f_1(\alpha) = \int_{\mu kT}^{E_{Cd}} \frac{v_o}{v} \frac{E_1^{\alpha}}{E^{1+\alpha}} dE \qquad -4.7$

which can be easily evaluated for any value of α.

To evaluate $I_o(\alpha)$ from available nuclear data, use is made of the effective resonance energy $\bar{E}_r$ introduced by Ryves and Paul ([6] and defined as "The energy of a single resonance which gives the same resonance activation effect as the actual resonances for the isotope". It should be noted that according to this definition, $\bar{E}_r$ is a function

of α, Ahmad ([11] has shown however, that $\bar{E}_r$ is only weakly dependent on α (i.e. similar to $W'(\alpha)$)

$$I_o(\alpha) = g\sigma_o \left[\left(\frac{E_1}{\bar{E}_r}\right)^{\alpha} \left(\frac{I_o}{g\sigma_o} - f_2(0)\right) + f_2(\alpha) \right] \qquad -4.8$$

where I_o is the resonance integral for $\alpha = 0$ and

$$f_2(\alpha) = \int_{E_{Cd}}^{\infty} \frac{v_o}{v} \frac{E_1^{\alpha}}{E^{1+\alpha}} \, dE \qquad -4.9$$

is the 1/v contribution to the resonance integral and $f_2(0) = f_2(\alpha)\Big|_{\alpha=0}$

Combining equations 4.6 and 4.7 gives

$$A = \Phi_{th} g\sigma_o + \phi_e g\sigma_o \left[\frac{W'}{g} + f_1(\alpha) + \left(\frac{E_1}{\bar{E}_r}\right)^{\alpha} \left(\frac{I_o}{g\sigma_o} - f_2(0)\right) + f_2(\alpha) \right] \qquad -4.10$$

The equivalent expression for a cadmium-covered irradiation is given by

$$A_{Cd} = \phi_e g\sigma_o \left[\left(\frac{E_1}{\bar{E}_r}\right)^{\alpha} \left(\frac{I_o}{g\sigma_o} - f_2(0)\right) + f_2(\alpha) \right] \qquad -4.11$$

In deriving equations 4.10 and 4.11, Ahmad et al ([67] have neglected any effects due to self-shielding in the foil. Since this can only be done when using infinitely dilute foils, it is necessary to modify equations 4.10 and 4.11 to allow for self-shielding. This gives

$$A = G_{th} \Phi_{th} g\sigma_o + \phi_e g\sigma_o \left[\frac{W'}{g} + f_1(\alpha) + \left(\frac{E_1}{\bar{E}_r}\right)^{\alpha} \left(\frac{G_r I_o}{g\sigma_o} - f_2(0)\right) + f_2(\alpha) \right] \qquad -4.12$$

$$\text{and } A_{Cd} = \phi_e g\sigma_o \left[\left(\frac{E_1}{\bar{E}_r}\right)^{\alpha} \left(\frac{G_r I_o}{g\sigma_o} - f_2(0)\right) + f_2(\alpha) \right] \qquad -4.13$$

where G_{th} and G_r are the self-shielding factors as defined in Chapter

Three and it has been assumed that the self-shielding factors needed to premultiply W', $f_1(\alpha)$, $f_2(0)$ and $f_2(\alpha)$ are sufficiently close to unity to be ignored.

This is equivalent to saying that the 1/v part of the cross-section is low enough for the foil to be regarded as thin, and that there are no large sub-cadmium resonances (included in W'). This would not apply to some isotopes e.g. ^{239}Pu.

In this work, the effective cadmium cut-off energy is taken as $E_{Cd} = 0.55$ eV for a cadmium box with uniform wall thickness of 1 mm as recommended by the European American Nuclear Data Committee and reported by Goldstein et al([68].

As the cadmium cut-off energy is dependent on the thickness of the cadmium box used; if any irradiations are performed in cadmium boxes of less than 1 mm wall thickness, it is necessary to modify equation 4.13 to take the extra activation into account (since the new $E_{Cd} < 0.55$eV).

In order to do this, define analogous quantities to W' and $f_1(\alpha)$.

$$W'' \equiv \frac{1}{\sigma_o} \int_{E_{Cd}}^{0.55} \left(\sigma(E) - \frac{g\sigma_o v_o}{v}\right) \frac{E_1^{\alpha}}{E^{1+\alpha}}\, dE \qquad -4.14$$

$$f_1''(\alpha) \equiv \int_{E_{Cd}}^{0.55} \frac{v_o}{v} \frac{E_1^{\alpha}}{E^{1+\alpha}}\, dE \qquad -4.15$$

and the activation under cadmium is then given by

$$A_{Cd} = \phi_e g\sigma_o \left[\frac{W''}{g} + f_1''(\alpha) + \left(\frac{E_1}{E_r}\right)^{\alpha} \left[\frac{G_r I_o}{g\sigma_o} - f_2(0)\right] + f_2(\alpha)\right] \qquad -4.16$$

4.3 Experimental Procedure

In order to measure with any accuracy, the variables Φ_{th}, ϕ_e and α for an irradiation site, it is necessary to (a) measure the reaction rates for more than three elements so as to provide an overdetermined set of solutions to equation 4.12, and (b) select a set of detectors such that their effective resonance energy values cover as wide a range as possible.

Taking into consideration the above two points, and the number of different detector materials which are readily available commercially, it was decided to study the (n,γ) reaction for the detectors listed in Table 4.1.

For an (n,γ) reaction, the saturated activity per target atom, A to be used in equation 4.12 is given by:-

$$A = \frac{NM}{N_{AV}\theta P_\gamma m \varepsilon_\gamma SDCt_m} \qquad -4.17$$

where N is the net peak area of the photopeak corrected for losses due to deadtime, pulse pile-up and coincident summing.

S is the correction for saturation during irradiation (see Section 4.4)

C is the correction for decay during counting, where

$$C = \left[1 - \exp(-\lambda t_m)\right] \cdot (\lambda t_m)^{-1}$$

D is the correction for decay between irradiation and gamma counting, where $D = \exp(-\lambda t_d)$

N_{AV} is Avogadro's number

M is the atomic mass

TABLE 4.1 Detector Characteristics

NUCLIDE	THICKNESS ($mg\ cm^{-2}$)	σ_o (Barns)	$\Delta(\sigma_o)$	I_o (Barns)	$\Delta(I_o)$	$\bar{E}$ (eV)	G_{th}	G_r*	W	g
^{197}Au	42	98.8	0.3	1549	27	5.47	0.968	0.406	0.05005	1.0052
	48						0.965	0.385		
	49						0.964	0.383		
^{55}Mn (81.3% Mn-Cu)	32	13.3	0.2	13.70	0.18	412	0.990	0.923	0	1.0
	33						0.991	0.922		
^{65}Cu	114	2.17	0.03	2.27	0.08	452	1.0	0.967	0	1.0
^{115}In	26	161	3	2595	56	1.51	0.939	0.355	0.2953	1.0194
	40						0.914	0.294		
	41						0.913	0.288		
^{186}W	254	37.4	1.1	469.8	9.8	19.5	0.971	0.401	0	1.0
	262						0.970	0.398		
^{23}Na (NaCl)	368	0.530	0.004	0.3057	0.0046	3130	0.930	0.965	0	1.0
^{59}Co **	50	39.7	4.3	18.8	1.5	133	0.963	0.658	0	1.0
	51						0.962	0.653		

** For reaction $^{59}Co(n,\gamma)^{60m}Co$ * = Calculated from the resonance parameters (BNL-325 Third Edition)

θ is the natural isotopic abundance

P_γ is the gamma-ray emission probability.

ε_γ is the gamma-ray photopeak efficiency

m is the elemental mass

For each irradiation, the foil was first cleaned so as to remove any contamination which may have been present, and then mounted on the centre of the shelf at the "2 cm" position on the aluminium irradiation ladder. Only one foil was irradiated at a time so that there would not be any perturbation in the flux due to neighbouring foils.

However, since the flux level seemed to be reproducible over a period of days, it was possible to normalize all the foils from the different irradiations to a single flux (see Section 4.4).

The "2 cm" position was selected as the irradiation site on the grounds that the relative flux density in the vertical direction is a maximum, and the flux gradient in the horizontal direction is reasonably flat at this position (see Ryves ([6]).

This means that the foils were irradiated in the maximum flux for the demand level used, and the positioning of the foils on the "2 cm" position shelf, was not too critical.

The demand voltage level was set to 20 volts for all irradiations.

After an irradiation, the foil was γ- counted using the type of system as described in Section 2.2.1. Details of the system components are given in Table 4.2.

The photopeaks to be analysed were selected so that the S.N.A. method of analysis could be employed (i.e. all peaks were first checked

for doublets using an analytical fitting procedure) and were corrected for all losses as described in Chapter 2. The count-rates were also corrected for γ-self absorption in the foil (see Section 4.5).

The absolute activities without cadmium cover were measured for all seven isotopes listed in Table 4.1. The cadmium covered absolute activities for ^{197}Au and ^{55}Mn, were also measured. (Note: For foils irradiated under cadmium, the foil was placed in a tissue 'envelope' inside the cadmium box, so as to prevent any cadmium from "rubbing off" onto the foil).

Each activity was measured at least three times.

The weighted mean value for the activity and the variance of the mean were calculated using equation 4.18 and either 4.19 or 4.20 (whichever gave the larger value) respectively:

$$\bar{x} = \frac{\sum_{i=1}^{N} \left(\frac{x_i}{\sigma_i^2}\right)}{\sum_{i=1}^{N} \left(1/\sigma_i^2\right)} \qquad -4.18$$

$$\sigma_\mu^2 = \frac{1}{\sum_{i=1}^{N} \left(1/\sigma_i^2\right)} \qquad -4.19$$

$$\sigma_\mu^2 \simeq \frac{1}{N(N-1)} \sum_{i=1}^{N} (x_i - \bar{x})^2 \qquad -4.20$$

where x_i is the i^{th} value

σ_i is the error on the i^{th} value

N is the number of measurements.

The σ_i were determined from the errors on

a) the γ-ray net-peak areas and

b) the correction factors described in Chapter two.

Equations 4-19 and 4.20 are sometimes referred to as the internal and external errors respectively.

Table 4.2 Details of Pulse-Height Analysis System

Component	Make	Remarks
DETECTOR	APTEC NRD (PHYGE)*	GEOMETRY:CLOSED-END COAXIAL
	CS/O-B31C(1.8)	ACTIVE AREA: 18.5 cm^2
	*PASSIVATED HYPER-PURE GERMANIUM DETECTOR	F.W.H.M. at 1.33 MeV:1.730 keV
		BIAS : + 2.5 kV
PREAMPLIFIER	CANBERRA 1413	
MAIN AMPLIFIER	TENNELEC TC 222	LINEAR AMPLIFIER
MULTICHANNEL ANALYSER	NUCLEAR DATA ND66	
FAST DISCRIMINATOR	ORTEC 420	TIMING SINGLE CHANNEL ANALYSER
PULSE SHAPING CIRCUITRY	EG&G MULTIPULSER, WIDTH/DELAY EG&G MULTIPULSER, OUTPUT	
RECYCLING PRESET SCALER	TWO CYCLE COUNTERS (N.P.L.)	
SCALER NO. 1	EG&G SCALER 226A	
REFERENCE PULSER + DELAY	BNC PULSE GENERATOR PB-4	

4.4 Correction for Saturation During Irradiation

If a foil is irradiated in a constant flux ϕ, for a time t_{irr}, then the activity of the foil at the end of the irradiation is given by

$$A = N\sigma\,\phi\,(1-e^{-\lambda\, t_{irr}}) \qquad -4.21$$

where the factor $(1-e^{-\lambda\, t_{irr}})$ is the correction for decay during irradiation.

However, in practice this is not the situation and the flux may vary with time.

The correction for saturation during irradiation is then calculated as follows (Ryves ([69]):

Consider the flux to vary as in Fig. 4.3

Fig. 4.3

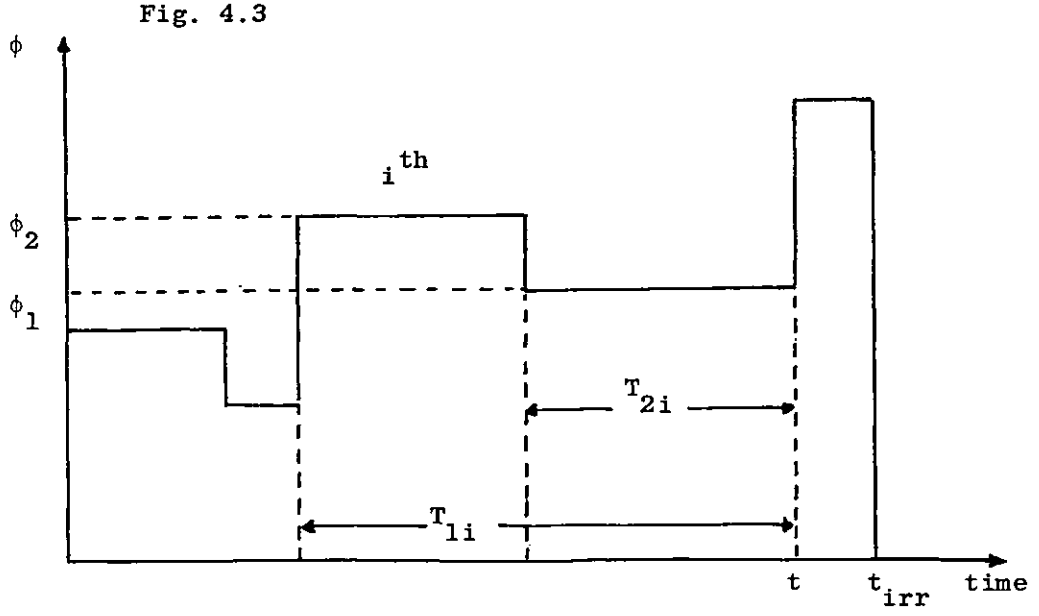

and consider the i^{th} and i^{th} + 1 intervals of time.

The activity of the foil at time t after being irradiated for a time T_{1i} is given by;

$$A(t) = N\sigma \{ \phi_1 (1-e^{-\lambda T_{2i}}) + \phi_2 (1-e^{-\lambda(T_{1i}-T_{2i})}) e^{-\lambda T_{2i}} \}$$

$$A(t) = N\sigma \{ \phi_2 (e^{-\lambda T_{2i}} - e^{-\lambda T_{1i}}) + \phi_1 (1-e^{-\lambda T_{2i}}) \}$$

or $A(t) = N\sigma \bar{\phi} f$

where $\bar{\phi}$ is the mean flux given by

$$\bar{\phi} = \frac{\sum_i \phi_i \Delta T_i}{\sum_i \Delta T_i}$$

and ΔT_i = Small interval of time over which flux is constant (e.g. T_{2i}) and f is the correction factor for decay during saturation.

Now a measure of the flux in any interval of time ΔT_i can be obtained from the number of counts accumulated in a neutron counter during the same interval of time.

i.e. $\phi_i = \frac{KC_i}{\Delta T_i}$ where K = A constant (assuming that the counter is stable over long periods of time)

C_i = number of counts in detector in i^{th} interval of time.

Therefore in the above case for the i^{th} and i^{th} + 1 intervals,

$$\bar{\phi} = K \frac{(C_1+C_2)}{\Delta T_1 + \Delta T_2}$$

In general, for all intervals of time up to t_{irr}

$$A(t_{irr}) = N\sigma \left[\sum_{\substack{i=all \\ intervals}} (e^{-\lambda T_{2i}} - e^{-\lambda T_{1i}}) \frac{C_i}{\Delta T_i} \right] \bar{\phi} \left(\frac{T_{irr}}{\sum_i C_i} \right)$$

or $A(t_{irr}) = N\sigma \bar{\phi} F_t (1-e^{-\lambda t_{irr}})$ -4.22

$$\text{and} \quad F_t = \frac{\left[\sum_i (e^{-\lambda T_{2i}} - e^{-\lambda T_{1i}}) \frac{C_i}{\Delta T_i}\right] T_{irr}}{\sum_i (C_i)\ (1-e^{-\lambda t_{irr}})} \qquad -4.23$$

For a constant flux, $\bar{\phi} \equiv \phi$, $F_t = 1.0$ and eq$^{ns.}$ 4.21 and 4.22 are identical.

When performing an irradiation, the length of each counting interval is set to approximately 1/15 of the half-life of the shortest lived nuclide being irradiated.

In the graphite-pile experiment, because the variations in flux are so small, it was possible to use the neutron counter output to normalize all irradiations to the same mean flux value.

4.5 Gamma Self-Absorption in Foils

As there are usually appreciable self absorption effects in most γ-ray sources, due to interactions suffered by primary photons whilst emerging from within the source, it is necessary to correct measured count rates to allow for this effect. It has been shown([70,71] that the photon emission at the surface of a flat source as reduced by self-absorption, is given by the approximate formula:

$$F = \frac{1 - e^{-\frac{\mu}{\rho} .D}}{\frac{\mu}{\rho} .D} \qquad -4.24$$

where F is the fraction of emitted photons

$\frac{\mu}{\rho}$ is the mass attenuation coefficient in $cm^2 g^{-1}$

D is source thickness in gcm^{-2}

Using expression 4.24, all low energy photon measurement data were converted to zero self-absorption. The mass attenuation coefficients were obtained by interpolating between the available lit-

erature values ([72] [74]).

For an absorber whose bulk density is ρ, and which is made up of a mixture of elements whose mass attenuation coefficients are

$\left(\frac{\mu_1}{\rho_1}\right)$, $\left(\frac{\mu_2}{\rho_2}\right)$,...., the overall mass attenuation coefficient is given by

$$\frac{\mu}{\rho} = \frac{\mu_1}{\rho_1} w_1 + \frac{\mu_2}{\rho_2} w_2 + \ldots\ldots$$

where w_1, w_2,..., are the fractions by weight of the elements which make up the absorber. Because the chemical binding energies between atoms in a molecule are very small, chemical compounds can be treated as mixtures ([72]).

The error in F is propagated in the normal manner.

$$\text{i.e.} \quad (\Delta F)^2 = \left(\frac{dF}{d\frac{\mu}{\rho}}\right)^2 (\Delta\frac{\mu}{\rho})^2 + \left(\frac{dF}{dF}\right)^2 (\Delta D)^2$$

For the graphite-pile experiment, 1/F correction factors varied between 1.0005 and 1.035.

4.6 The Calculation of W'

The non-1/v part of the resonance activity produced by neutrons between the effective cadmium cut-off energy E_{Cd} and the epithermal cut-off energy E_c, is given by means of the quantity W' :

$$W' = \frac{1}{\sigma_o} \int_{E_c}^{E_{Cd}} \left[\sigma_a(E) - g\sigma_o \left(\frac{E_o}{E}\right)^{\frac{1}{2}}\right] \frac{dE}{E} \qquad -4.25 .$$

It is assumed that only the lowest principal resonance departs

from a $1/\sqrt{E}$ energy dependence between the limits of integration. Using the single level Breit-Wigner formula for this resonance, the integral can be evaluated numercially (using the Simpson's rule technique). It was found that only the W' values for Au and In were significant and were calculated assuming $E_c = 0.13eV$, $E_{Cd} = 0.55eV$ and $T = 20^oC$. The values obtained were $W'_{Au}{}^{197} = 0.05005$ and $W'_{In}{}^{115} = 0.2953$.

In equation 4.25 the factors for resonance self-shielding G_r, and the transmission of resonance neutrons through cadmium F, have been omitted since they are both close to unity, and it is assumed that $W' = W'G_rF$.

4.7 Determination of Flux Parameters

In order to estimate the three flux parameters Φ_{th}, ϕ_e and α for an irradiation site, it is necessary to measure either (a) cadmium ratios of two or more isotopes to estimate $\frac{\Phi_{th}}{\phi_e}$ and α, (b) cadmium covered absolute activities of at least two isotopes to estimate ϕ_e and α, or (c) absolute activities without cadmium cover of at least three isotopes to obtain all three parameters.

Methods (b) and (c) are employed in this work with method (b) providing the best determination of the epithermal flux parameters.

The method used to estimate the flux parameters using equations 4.12 or 4.13 and 4.17, is the generalised least squares method, which requires more measured quantities than the minimum numbers referred to above in order to produce an over-determined set of simultaneous equations. In this method, the measured quantities can be written as a vector $[E]$, with its associated variance-covariance

matrix $[V_e]$. The data in $[E]$ are to be compared with the predictions of the model as described by equations 4.12, 4.13 and 4.17. These predictions, which form a vector $[C]$, depend on the parameters, $[P_o]$, used in the model, including both nuclear data and flux parameters. The best estimates of these and their associated variance-covariance matrix are obtained by minimizing chi-squared:

$$\chi^2 = [P_1-P_o]^T [V_p]^{-1} [P_1-P_o] + [E-C]^T [V_e]^{-1} [E-C] \qquad -4.26$$

in which the symbol T represents the transpose of a matrix and -1 the inverse. $[P_1]$ is a vector containing prior information about the parameters and $[V_p]$ is the variance-covariance matrix for $[P_1]$.

The iterative search procedure to find the values of P_o which minimize chi-squared was carried out using the CERN library code MINUIT, as modified for this problem by Ahmad and Williams ([67]. A more full description of the program and its use, is given by Ahmad ([11].

4.8.1 Input Data

Five items of nuclear data are needed to predict the measured gamma emission rates: η, $\frac{G_r I_o}{g\sigma_o}$, $\bar{E}_r$, $\frac{W'}{g}$ and the decay constant λ. Where η is a compound nuclear data parameter defined by:

$$\eta = \theta P_\gamma \, g\sigma_o \, M^{-1} \qquad -(1)$$

and θ is the mole fraction of the target isotope

P_γ is the emission probability of the relevant γ-ray

M is the atomic mass.

Only η and $\frac{G_r I_o}{g\sigma_o}$ contribute significantly to the total uncertainty

of the activities, with the main uncertainty in η coming from the values for P_γ and σ_o.

The other items, therefore, can be treated as known constants and the values taken from the literature ([75-78]).

The initial* values of P_γ and their standard deviations were taken from** the Table of Isotopes ([75]). (*: see section on results and conclusions). (** In the case of ^{187}W, P_γ values were taken directly from Zijp and Baard ([80]).

Since there is often a large scatter in quoted I_o values, it was decided to perform an evaluation in order to determine the most likely value. (see Section 4.8.2). σ_o values were either evaluated in a similar way, or in cases when no recent data were available, taken from BNL-325 ([76]).

G_r values were taken from the literature, if the literature values had been determined experimentally, otherwise were calculated from the resonance parameters ([76]) using the Monte-Carlo code described in Chapter Three.

The resulting values of η and $\frac{G_r I_o}{g\sigma_o}$ with their uncertainties form part of the prior information contributing to $[P_1]$ and $[V_p]$. The remaining values appearing in $[P_1]$ are initial estimates of the flux parameters Φ_{th}, Φ_e and α. Since these are poorly known the corresponding variances are taken to be very large and this ensures that the solution parameters $[P_o]$ are not influenced by them. (All the input data used are listed in Table 4.3).

The input vector $[V_p]$ was assumed diagonal.

4.8.2 Evaluation of I_o

The recent compilation of I_o, by Gryntakis and Kim (1980) ([79]) has a very large scatter for many isotopes.

The values for the same isotope may differ from one another by more than the standard deviation claimed for each measurement. An evaluation was therefore necessary to determine the most likely value. First of all, only those values for which errors were cited were considered for the evaluation. Secondly, it was decided to omit any calculated values on the grounds that it is not always evident what the errors quoted with them represent (i.e. 1σ, 3σ, an upper limit, etc).

Although the result of an evaluation based only on measured data may be biased due to some of the data not being determined in an $\alpha = 0$ slowing down spectrum, it is assumed that the evaluation method used, will reject the worst cases, and that the weighted mean of all the other data is close to the true value of $I_o(0)$.

The evaluation method used was to take a weighted mean of all the experimental data using equations 4.18 and 4.19, and provided these data passed a chi-squared two-tailed test at the 5% significance level, then the best estimate value was accepted. If the chi-squared test failed then the individual contributions to the chi-squared value were studied to reveal any outliers. Any measurements which were discrepant from the weighted mean of the remaining values by more than three standard deviations were then excluded from the evaluation, (provided the remaining values passed the chi-squared test).

This type of evaluation has also been described by Ahmad ([11]

4.9 Results and Conclusions

When the consistency analysis was applied to the experimental data and the input nuclear data described in Section 4.8.1, the value of χ^2 obtained (see equation 4.26) failed a two-tailed test even at a 99.95% confidence level indicating that there were severe inconsistencies in the data. It was observed however, that the major contributions to χ^2 arose from the η values for indium and tungsten, which implicates the P_γ values as the probable source of the inconsistencies. Other sets of P_γ data were then tested and the set of data shown in Table 4.4 when included in the consistency analysis, gave a value of χ^2 of 43 for 36 degrees of freedom which passed the two-tailed test at the 95% confidence level. In Table 4.4 the P_γ values for ^{116m1}In were taken again from the Table of Isotopes but were the third set given therein (with reference code RRL-16-241(74)) rather than the first, recommended, set. In the case of ^{187}W the P_γ data were taken directly from Brenner and Meyer ([81]).

The P_γ values for indium and tungsten given in Table 4.4 are in good agreement with those recommended independently by De Corte et al. (1982) ([82]).

If the P_γ values for indium given in Table 4.3 are compared with those given in Table 4.4, it can be seen that the difference in values at 417 keV is significantly greater than at any other energy. It should also be noted that the output η value from the consistency analysis, implies that this discrepancy is even larger.

This result is in agreement with some work done by W. Taylor (Winfrith 1982) ([83]) on the decay scheme of indium, in which Taylor concludes

TABLE 4.3 Initial Input Nuclear Data

Target	σ_o barns	I_o	$I_o/g\sigma_o$	E_γ keV	P_γ	$\bar{\eta}$ barn.mol. kg^{-1}
^{23}Na	0.530 ± 0.004	0.306 ± 0.005	0.577 ± 0.010	1368	1.00	23.05 ± 0.18
^{55}Mn	13.3 ± 0.2	13.70 ± 0.18	1.03 ± 0.02	847	0.9887 ± 0.0004	239 ± 4
^{59}Co	18.8 ± 1.5	39.7 ± 4.3	2.1 ± 0.3	59	0.020 ± 0.001	6.4 ± 0.6
^{65}Cu	2.17 ± 0.03	2.27 ± 0.07	1.05 ± 0.04	1039	0.08 ± 0.01	0.84 ± 0.11
^{115}In	161 ± 3	2595 ± 56	15.8 ± 0.5	138	0.033 ± 0.002	45.6 ± 2.9
				417	0.324 ± 0.015	443 ±22
				819	0.116 ± 0.006	159 ± 9
				1097	0.557 ± 0.015	762 ±25
				1294	0.85 ± 0.02	1163 ±35
				1507	0.102 ± 0.005	140 ± 7
^{186}W	37.4 ± 1.1	470 ± 10	12.56 ± 0.45	480	0.234 ± 0.010	13.6 ± 0.7
				512	0.0069 ± 0.0006	0.40 ± 0.04
				619	0.067 ± 0.003	3.9 ± 0.2
				626	0.0117 ± 0.0005	0.68 ± 0.04
				686	0.293 ± 0.012	17.0 ± 0.9
				773	0.0442 ± 0.0018	2.57 ± 0.13
^{197}Au	98.8 ± 0.3	1549 ± 27	15.60 ± 0.27	412	0.955 ± 0.001	481.5 ± 1.6

TABLE 4.4 Revised Input Data and Output η Values

Target	E_γ keV	P_γ	Input η	Output η
^{23}Na	1368	1.00	23.05 ± 0.18	22.83 ± 0.16
^{55}Mn	847	0.9887 ± 0.0004	239 ± 4	233 ± 2
^{59}Co	59	0.020 ± 0.001	6.4 ± 0.6	6.86 ± 0.10
^{65}Cu	1039	0.08 ± 0.01	0.84 ± 0.11	0.87 ± 0.03
^{115}In	138	0.0330 ± 0.0014	45 ± 2	50.8 ± 0.6
	417	0.278 ± 0.012	380 ± 18	370 ± 4
	819	0.116 ± 0.005	159 ± 7	164.6 ± 2.0
	1097	0.573 ± 0.022	784 ± 34	786 ± 8
	1294	0.846 ± 0.020	1157 ± 35	1139 ± 14
	1507	0.107 ± 0.005	146 ± 7	137 ± 3
^{186}W	480	0.253 ± 0.005	14.7 ± 0.5	15.4 ± 0.2
	512	0.00747± 0.00017	0.435± 0.016	0.468± 0.006
	619	0.0727 ± 0.0014	4.23 ± 0.15	4.36 ± 0.04
	626	0.0126 ± 0.0003	0.733± 0.027	0.755± 0.008
	686	0.316 ± 0.007	18.4 ± 0.7	18.9 ± 0.2
	773	0.0477 ± 0.0010	2.78 ± 0.10	2.85 ± 0.03
^{197}Au	412	0.955 ± 0.001	481.5 ± 1.6	481.7 ± 1.6

that the 417 keV branching ratio may not be as well known as it is claimed to be. His results suggest that the branching ratio is equal to Lederer's recommended value multiplied by 0.80 ($\pm$ 6%), i.e. $P_\gamma = 0.259 \pm 0.020$, which is in good agreement with the results obtained from the consistency analysis.

The ability of the consistency analysis to improve knowledge of nuclear data can be seen by comparing the precision of the input and output values of η in Table 4.4. The improvement in precision being often by a factor of three or more. This means a factor of approximately 10 in the variance. In terms of information content this means that 90% of the information in the output data was new and absent from the input data. It should be noted that the output values are highly correlated with one another and their variance-covariance matrix is given in Appendix II.

The output of the consistency analysis also contains the three flux parameters for the irradiation position used. A comparison of the values obtained in this experiment, with the previous measurements in the same position reported by Ryves and Paul ([6] (1968) is given in Table 4.5

TABLE 4.5 Flux parameters for the "2 cm" Irradiation Position in the N.P.L. Graphite-pile

Flux parameter	This experiment	Ryves and Paul
Φ_{th} [n cm^{2}s^{-1}]	$(1.259 \pm 0.009) \times 10^7$	$(1.272 \pm 0.012) \times 10^5$
ϕ_e [n cm^{2}s^{-1}]	$(1.42 \pm 0.05) \times 10^5$	-
ϕ_e/Φ_{th}	$(1.12 \pm 0.04) \times 10^{-2}$	$\leqslant 1.0 \times 10^{-2}$
α	0.048 ± 0.010	0.049 ± 0.001

Although the values for the thermal and epithermal flux components are slightly different, the agreement between the values is still very good. The slight difference in values may be due to the fact that since Ryves and Paul performed their experiment; (a) the original accelerator beam line in the graphite-pile has been replaced by one which has slightly thicker walls, (this would cause a drop in the flux) and (b) the standard resistor used in the demand-level voltage network has been changed slightly. This means that there will be a slightly different flux to demand-level relationship to that measured by Ryves and Paul.

At first sight it appears that although the α values are in good agreement, the error quoted for the value measured in this experiment is a factor of ten more than that reported by Ryves and Paul. It is believed that this discrepancy in precision is due to Ryves and Paul neglect of any variations in the nuclear data when performing the error propagation for α. If these variations are taken into account it can be shown ([84]that the error quoted for α as measured in this experiment is in fact more realistic.

CHAPTER FIVE

Calibration of the N.P.L. Standard Slowing-Down neutron Spectrum Facility

In the standard slowing-down neutron spectrum facility at the National Physical Laboratory, the flux parameter α is believed to be zero, (i.e. the spectrum is of the form 1/E). This flux facility can, therefore, be used for the fundamental determination of resonance integrals. The purpose of this experiment is (a) to calibrate foil detectors in this 1/E flux facility and simultaneously gain improved knowledge of the resonance integrals for the isotopes used in the calibration, and (b) to test further, the validity of the neutron flux convention described in Section 4.2.

By use of the (n,γ) reaction, experimental activation data for the isotopes ^{197}Au, ^{55}Mn and ^{158}Gd were used for the calibration, and best-estimates of the flux parameter ϕ_e and the input nuclear data were obtained by using the least-squares minimization technique described in Chapter four.

This chapter contains details of the experiment (including a brief description of 4π β-γ coincidence counting) and discusses the importance of the output nuclear data values obtained from the consistency analysis.

5.1 N.P.L. Standard Slowing-down Neutron Spectrum Facility

A schematic diagram of the N.P.L. standard 1/E flux facility is shown in Fig. 5.1. A slowing-down epithermal neutron flux is obtained from the moderation of fast neutrons in water. The neutrons are produced by a magnetically analysed beam of deuterons from a Van de Graaff accelerator impinging on a thick beryllium metal target (similar to Section 4.1). The target is positioned at the centre of a large cylindrical

Fig. 5.1 A Schematic Diagram of the Standard 1/E Flux Facility

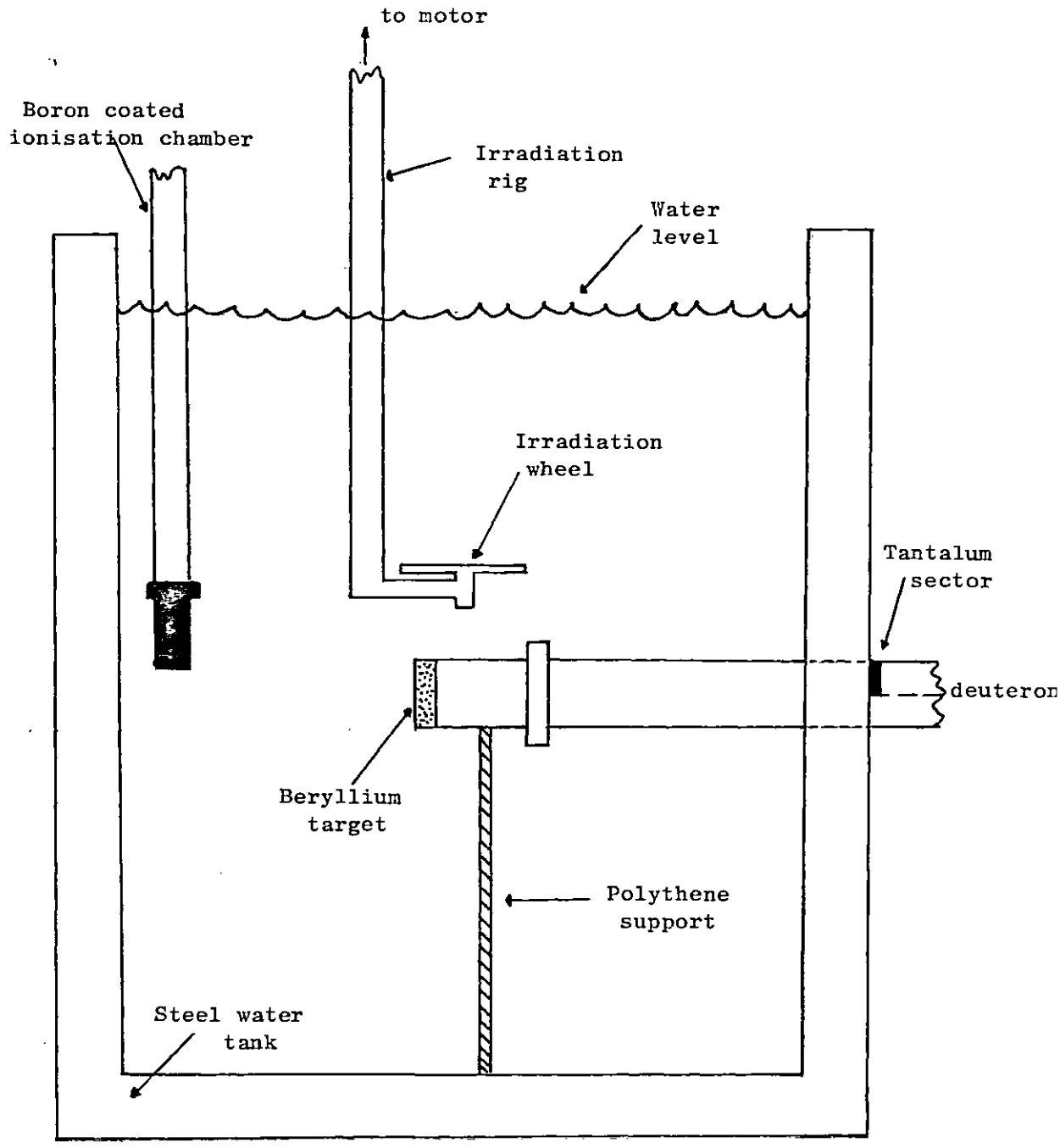

water tank (height 2.4m, diameter 2m) and is water cooled to prevent any damage. The thermalized neutron flux density in the water towards the edge of the tank can be continuously monitored with a boron-coated ionization chamber. The output from the ionization chamber enables the target output to be held constant to within 2% by a servo-system. The irradiation rig is mainly constructed from thin perspex in order to help minimize the perturbations due to displaced water. Up to eight circular foils can be irradiated simultaneously in each measurement.

The foils are positioned at equal distances on the circumference of a 14 cm diameter circle and encased in a thin perspex wheel which rotates in the horizontal plane at 140 r.p.m. This technique is necessary because of the large gradient in the flux and ensures that each foil of equal area has an equal average irradiation.

5.2 $4\pi\beta$-γ Coincidence Counting

Coincidence counting is widely used to measure the absolute disintegration rate of nuclides which decay by the emission of two radiations in cascade.

The $4\pi\beta$-γ coincidence technique is used to measure the absolute disintegration rate of radionuclides which decay by the emission of a β- particle and a coincident γ-ray. The counting system usually comprises a 4π gas flow proportional beta counter, with methane or argon/methane as counting gas and two sodium iodide crystals as gamma detectors positioned on either side of the proportional counter. In the measurement of the absolute disintegration rate of a source, N_o, which decays by the emission of a β- particle and coincident γ-ray; a coincidence is

only recorded when the β and γ-rays from the same disintegration are simultaneously detected in their respective counters.

Assuming that the γ-detector has an efficiency ε_γ and the β-detector has an efficiency ε_β, then the recorded count rates are given by:

$$\gamma\text{- count rate, } N_\gamma = N_o \varepsilon_\gamma \qquad - 5.1$$

$$\beta\text{- count rate, } N_\beta = N_o \varepsilon_\beta \qquad - 5.2$$

$$\text{coincidence count rate, } N_c = N_o \varepsilon_\beta \varepsilon_\gamma \qquad - 5.3$$

$$\text{Thus} \quad N_o = \frac{N_\beta N_\gamma}{N_c} \qquad - 5.4$$

$$\text{and } \varepsilon_\beta = \frac{N_c}{N_\gamma}$$

It is necessary however, to make corrections to these equations to allow for:

(i) deadtime in the β- and γ-channels and random coincidences

(ii) the γ-sensitivity of the β-detector

(iii) the β-sensitivity of the γ-detector

(iv) conversion electrons

(v) β-γ angular correlation

When the decay scheme involves complex β- and γ- branching, 5.1, 5.2 and 5.3 must be further modified. These modifications have been discussed by Campion ([85].

For coincidence measurements on a nuclide with a decay scheme involving n different β- branches, each of which may be followed by prompt γ-emission, the observed count rates for the three channels are given by the following equations ([86]:

$$N_\beta = N_o \sum_{r=1}^{n} a_r \left\{ \varepsilon_{\beta r} + (1-\varepsilon_{\beta r}) \left[\frac{\alpha \varepsilon_{ce} + \varepsilon_{\beta\gamma}}{1+\alpha} \right]_r \right\} \qquad -5.5$$

$$N_\gamma = N_o \sum_{r=1}^{n} a_r \frac{\varepsilon_{\gamma r}}{1+\alpha_r} \qquad -5.6$$

$$N_c = N_o \sum_{r=1}^{n} a_r \left\{ \frac{\varepsilon_{\beta r}\varepsilon_{\gamma r}}{1+\alpha_r} + (1-\varepsilon_{\beta r})\varepsilon_{cr} \right\} \qquad -5.7$$

For the r^{th} branch

a_r = the fractional intensity

$\varepsilon_{\beta r}$ = the β-detection efficiency

α = the total internal conversion coefficient associated with this β-branch

ε_{ce} = β-detector efficiency for these conversion electrons

ε_{cr} = probability of recording a coincidence when the associated β-particle is not detected.

$\varepsilon_{\gamma r}$ and $\varepsilon_{\beta r}$, respectively, are efficiencies of the γ- and β-detectors for γ-rays associated with the r^{th} branch.

Equation 5.4 can now be rewritten as

$$\frac{N_\beta N_\gamma}{N_c} = N_o (1 + k) \qquad -5.8$$

where the correction (1 + k) depends on the variations of the efficiency of each detector between different branches of the decay scheme. The quantities on the right hand side of equations 5.5, 5.6 and 5.7 are usually very difficult to determine accurately.

Baerg ([86], however, has shown that solutions to these equations can be in one of several unspecified general forms:

$$\frac{N_\beta N_\gamma}{N_c} = N_o G \left(\frac{N_\gamma}{N_c}\right) \qquad - 5.9$$

$$N_\beta = N_o F \left(\frac{N_c}{N_\gamma}\right) \qquad - 5.10$$

The functions G and F $\rightarrow$ 1 as $\frac{N_\gamma}{N_c}$ and $\frac{N_c}{N_\gamma} \rightarrow 1$, respectively.

One procedure of measuring N_o, therefore, is to measure N_β, N_γ and N_c for various values of ε_β, and plot a graph of either $\frac{N_\beta N_\gamma}{N_c}$ vs $\frac{N_\gamma}{N_c}$ or N_β vs. $\frac{N_c}{N_\gamma}$ and perform an extrapolation to $\frac{N_\gamma}{N_c} = 1$.

It is obvious that it is necessary to have as high a β-detector efficiency as possible so that the extrapolations will only be over a short range. The general basis of the $4\pi\beta$-γ coincidence technique and a description of the correction factors required when using it have been well documented ([85,86] elsewhere.

5.3 Experimental Procedure

In order to calibrate the 1/E standard flux facility with any accuracy, it is desirable to measure the reaction rates for more than the minimum number of isotopes required to solve equations 4.12 or 4.13 so as to provide an overdetermined set of solutions to these equations. In order to also gain improved knowledge of the resonance integrals for the isotopes used in the calibration, it was decided that the maximum amount of information (in the time available) would be gained if all the measurements were performed under cadmium. The only extra information which would be gained if bare irradiations were made, would be on Φ_{th} and σ_o. The minimum number of isotopes needed for the calibration, therefore, was two. Although this chapter reports the calibration in

terms of only three isotopes ^{197}Au, ^{55}Mn and ^{158}Gd, (i.e. equation 4.13 is only over-determined by one isotope) in fact seven different elements were irradiated. Due to unavoidable experimental difficulties however, the results for four of the elements were unreliable and have therefore not been included in the analysis. This is because any bias in the experimental measurements would be reflected in the output values from the consistency analysis. For each irradiation, eight foils in 1mm thick cadmium boxes were irradiated simultaneously in a thin perspex wheel as described in Section 5.1. The rotational speed of the wheel was first checked for any fluctuations, and was found to be constant at 140 r.p.m. $\pm$ 0.3%. The irradiation rig was placed so that the foils were close to the beryllium target but immediately above it. This was done so that the foils would be irradiated in the maximum flux with as small a flux gradient as possible. Before an irradiation, each foil was first cleaned so as to remove any contamination, and then placed in a tissue envelope to prevent any cadmium from rubbing-off onto the foil.

The absolute disintegration rates of all the irradiated foils, except manganese, were determined at The Reactor Centre, Imperial College, using a $4\pi\beta$-γ coincidence system which has been described in detail elsewhere by Olomo ([87]). The beta detector was operated in the proportional region at a pressure slightly above atmospheric, with 90% Ar/ 10%CH_4 as the counting gas. By using a linear gate, linear delay and an oscilloscope, the thresholds and window widths in the gamma channels were set, and for each isotope the gamma window was gated on a prominant photopeak in the spectrum of the isotope. The quantities N_β, N_γ and N_c (see Section 5.2) were determined for various values of the beta channel low-level discriminator. Increasing the beta channel low-level discriminator

in effect reduces the beta channel efficiency which is given, to first order, by $\frac{N_c}{N_\gamma}$. The variation of the beta efficiency was performed over 16 discriminator levels. Both the relationships given by equations 5.9 and 5.10 were used for the determination of N_o. The functions F and G were found to be linear or to have very small quadratic terms.

The total disintegration rate for each foil was determined from the extrapolation values resulting from the fits of $\frac{N_\beta N_\gamma}{N_c}$ vs. $\frac{N_\gamma}{N_c}$ and N_β vs. $\frac{N_c}{N_\gamma}$ as calculated using the program COADERT ([87]. The efficiency extrapolation technique has been described by Baerg ([88].

The manganese foils were counted on a $4\pi\beta$-γ coincidence system at the N.P.L. From equation 5.8 it can be seen that the coincidence equation for manganese can be written as

$$N_o = \frac{N_\beta}{\left(\frac{N_c}{N_\gamma}\right)(1 + k_{Mn})} \qquad - 5.11$$

where k_{Mn} is a correction factor which depends upon the β-detector efficiency, the γ-sensitivity of the β-detector and the number of γ-γ coincidences.

Since the variation of k_{Mn} vs. ε_β is very well known for the N.P.L. coincidence system, the values N_β, N_γ and N_c were measured several times at the maximum possible beta detector efficiency, and the appropriate k_{Mn} correction factor, for the beta efficiency measured, looked up in tables and applied in equation 5.11.

All count rates were corrected for accidental coincidences, deadtime losses, background, decay between irradiation and counting and decay during counting. The count rates were also corrected for saturation

during irradiation in the same manner as described in Section 4.4, except that because the flux in the standard 1/E flux facility is not as reproducible as in the thermal flux facility, it was decided not to normalize irradiations done on different days to a single irradiation. Each isotope was measured at least three times. Some of the absolute count rates measured had errors larger than those normally associated with $4\pi\beta$-γ coincidence counting, caused by the low β-detector efficiency values encountered when using thick foils, hence the large extrapolations necessary to determine N_o.

For an (n,γ) reaction, the saturated activity per target atom, A_{Cd} to be used in equation 4.13 is given by:

$$A_{Cd} = \frac{N_o \cdot M}{N_{AV} \cdot \theta \cdot m \cdot F_{Cd}} \qquad - 5.12$$

where N_o is the corrected absolute disintegration rate (per sec)

M is the atomic mass

N_{AV} is Avogadro's number

m is the elemental mass

θ is the natural isotopic abundance

F_{Cd} is the cadmium epithermal neutron transmission factor.

The cadmium epithermal neutron transmission factor, F_{Cd}, accounts for the fact that the specific count rate A_{Cd}, of a cadmium covered isotope is, in some cases, significantly different from A, the specific count rate of the bare isotope induced by epithermal neutrons. F_{Cd} is defined ([89] as: $F_{Cd} = \frac{A_{Cd}}{A}$

Usually F_{Cd} factors do not significantly differ from unity. However, when the resonances of Cd and of the Cd-covered isotope partially overlap,

F_{Cd} can be markedly lower than unity, (e.g. $^{186}W(n,\gamma)^{187}W$). F_{Cd} values can also be higher than unity if neutrons, which are resonance scattered in the cadmium, enter the correct energy band to be resonantly captured in the Cd-covered isotope (e.g. $^{65}Cu(n,\gamma)^{66}Cu$).

Combining equations 4.13 and 5.12 gives

$$\frac{N_o}{m \cdot F_{Cd}} = N_{AV}\, \theta g \sigma_o M^{-1}\, \phi_e \left[\left(\frac{E_1}{\bar{E}_r}\right)^{\alpha} \left(\frac{G_r I_o}{g\sigma_o} - f_2(0)\right) + f_2(\alpha) \right] \qquad - 5.13$$

The quantity $\frac{N_o}{m \cdot F_{Cd}}$ was calculated for all the foils.

5.4.1 Input Data

In order to carry out a consistency analysis of the measurements, it is first necessary to obtain from the available literature best values of nuclear data to be used as input for the analysis.

As given by equation 5.13, four items of nuclear data are needed to predict the measured absolute activities : Ω, $\frac{G_r I_o}{g\sigma_o}$, $\bar{E}_r$ and the decay constant λ.

Where Ω is a compound nuclear data parameter defined by $\Omega \equiv \theta g \sigma_o M^{-1}$ (symbols are defined in Section 4.8.1). Only Ω and $\frac{G_r I_o}{g\sigma_o}$ contribute significantly to the total uncertainty of the activities, with the main uncertainty in Ω coming from the value of σ_o.

The other items can be treated as known constants and the values taken from the literature ([76,77,78]).

The epithermal neutron transmission factors, F_{Cd} used for ^{197}Au and ^{55}Mn were those recommended by T. El Nimr et al. (1981) ([89]). The F_{Cd} value for ^{158}Gd was assumed to be 1.0 on the grounds that there is

a negligible amount of overlap between the gadolinium and cadmium resonances. The I_o and σ_o values were evaluated from the literature ([76,10] using the procedure described in Section 4.8.2 and the resonance self-shielding factors, G_r were calculated from the resonance parameters ([76] using the Monte-Carlo code described in Chapter three.

Table 5.1 contains details of the input nuclear data

5.4.2 Correlations in the Input Parameters

The presence of the term $g\sigma_o$ in both $\Omega = \theta g\sigma_o M^{-1}$ and $\frac{G_r I_o}{g\sigma_o}$, introduces correlations between these two values when they refer to the same isotope. The presence of the correlations implies that the appropriate off-diagonal terms must be calculated for the input variance-covariance matrix for the variable parameters. Assuming that the correlation is only due to the 2200 m/s cross-section then the covariances can be generated using equation 5.14 ([91]

$$\text{cov}\left(\Omega, \frac{G_r I_o}{g\sigma_o}\right) = -\Omega \frac{G_r I_o}{g\sigma_o} \left(\frac{\sigma(\sigma_o)}{\sigma_o}\right)^2 \qquad - 5.14$$

Proof

Let $y_1 = f_1(p_1, p_2, \ldots . p_n)$

$y_2 = f_2(p_1, p_2, \ldots . p_n)$

and let the parameters $p_1, p_2, \ldots p_n$ be independent of each other.

$$\text{Now } \delta y_1 = \frac{\partial y_1}{\partial p_1} \delta p_1 + \frac{\partial y_1}{\partial p_2} \delta p_2 + \ldots . + \frac{\partial y_1}{\partial p_n} \delta p_n$$

$$\text{and} \qquad \delta y_2 = \frac{\partial y_2}{\partial p_1} \delta p_1 + \frac{\partial y_2}{\partial p_2} \delta p_2 + \ldots . + \frac{\partial y_2}{\partial p_n} \delta p_n$$

$\text{cov}(y_1, y_2) = \langle \delta y_1 \, \delta y_2 \rangle$ where $\langle \ \rangle$ represents the expectation value.

TABLE 5.1 Initial Input Nuclear Data

Nuclide	Foil thickness ($mg\ cm^{-2}$)	G_r	σ_o (barns)	I_o (barns)	$\bar{E}_r$ (ev)	F_{Cd}	Ω $mol \cdot kg^{-1}$ barn	g
^{197}Au	47	0.388±.008	98.67±0.10*	1549±27	5.47	0.991	503.55±0.72	1.0052
	48	0.385±.008						
	49	0.383±.008						
^{55}Mn	13.2	0.948±.010	13.3 ±0.2	13.70±0.18	412	1.0	242.1 ±3.6	1.0
88% Mn/ 12% Ni	13.7	0.947±.009						
^{158}Gd	69	0.877±.008	2.5 ±0.5	74.8 ±3.3	45.4	1.0	3.93±0.79	1.0

* → value taken from reference 90.

$$= < \frac{\partial y_1}{\partial p_1} \quad \frac{\partial y_2}{\partial p_1} \quad \delta p_1^2 + \ldots\ldots\ldots \text{(similar terms)}$$

$$+ \quad 2 \quad \frac{\partial y_1}{\partial p_1} \quad \frac{\partial y_2}{\partial p_2} \quad \delta p_1 \delta p_2 + \ldots\ldots \text{(similar terms)} + \ldots\ldots >$$

$$= \frac{\partial y_1}{\partial p_1} \quad \frac{\partial y_2}{\partial p_1} \quad <\delta p_1^2> + \ldots\ldots\ldots$$

$$+ 2 \quad \frac{\partial y_1}{\partial p_1} \quad \frac{\partial y_2}{\partial p_2} \quad <\delta p_1 \ \delta p_2> + \ldots\ldots\ldots$$

$$= \frac{\partial y_1}{\partial p_1} \quad \frac{\partial y_2}{\partial p_1} \quad \text{var } (p_1) \quad + \ldots\ldots\ldots$$

$$+ 2 \quad \frac{\partial y_1}{\partial p_1} \quad \frac{\partial y_2}{\partial p_2} \quad \text{cov } (p_1 \ p_2) + \ldots\ldots\ldots$$

Since $p_1, p_2, \ldots p_n$ are independent then all covariance terms are zero and,

$$\text{cov } (y_1, y_2) = \frac{\partial y_1}{\partial p_1} \quad \frac{\partial y_2}{\partial p_1} \quad \text{var } (p_1) + \ldots\ldots \text{(similar terms)} \qquad - 5.15$$

5.5 Results and Conclusions

The results from two separate irradiations are included in the analysis, with the consistency analysis being applied to the data from each irradiation separately. The reason for this is twofold: (a) as described in Section 5.3, it is not possible to satisfactorily normalize irradiations done on different days to a single irradiation and (b) although it would be better to treat the data from both irradiations as being from different irradiation sites and perform the consistency analysis on all of the data; problems encountered when using program MYMAIN ([11] (which calls MINUIT), however, make this not possible.

Although α is believed to be zero in the standard 1/E flux facility, it was decided to allow the variance on α (as well as that on ϕ_e) to be very large.

This ensures that the solution parameters $[P_o]$ are not influenced by the input values of either ϕ_e or α. This also allows several tests to be made, for if the consistency analysis gives output values for α which are significantly different from zero then one can conclude that either (a) The neutron flux model described in Chapter Four is inadequate.

(b) The spectrum in the standard slowing down neutron flux facility is not proportional to 1/E (i.e. $\alpha \neq 0$) or

(c) The input nuclear data used for the consistency analysis may be biased, (e.g. the evaluated I_o values may be biased due to some of the measurements included in the evaluations, not having been determined in an $\alpha = 0$ spectrum). This bias will then be reflected in the output value for α.

When the consistency analysis was applied to both sets of irradiation data and the input nuclear data described in Section 5.4.1, the value of χ^2 obtained, failed a two-tailed test even at a 99.95% confidence level, on both occasions. This indicated that there were again, severe inconsistencies in the data (c.f. the Thermal-Pile experiment). It was observed however, that in both cases the major contributions to χ^2 arose from the Ω and $\left(\frac{G_r I_o}{g\sigma_o}\right)$ values for gadolinium.

The output values for $\left(\frac{G_r I_o}{g\sigma_o}\right)_{Gd}$ indicated that the input value for I_o for gadolinium was far too low. A study of the resonance integrals for ^{158}Gd cited in Gryntakis & Kim([10] shows that the latest reported measurement by Steinnes ([92](1975) is significantly larger than the other

values cited, and infact supercedes an earlier measurement made by the same measurer. On these grounds it was decided to use Steinnes' value for the gadolinium resonance integral ($I_o = 127 \pm 38$). The gadolinium resonance self-shielding factor was recalculated accordingly ($G_r = 0.924 \pm 0.023$).

The results of the consistency analysis when this new gadolinium data is included, are shown in tables 5.2 and 5.3.

As can be seen from tables 5.2 and 5.3, on both occasions, the consistency analysis gives a value of χ_1^2 which passes the two-tailed test at the 95% confidence level.

The output values for α are both very small and consistent with zero. This is in agreement with the assumption that $\alpha = 0$ for this facility and confirms that this facility can be used to provide a standard 1/E spectrum. The output values of Ω are not significantly different from the input values. This is to be expected since the main uncertainty in the Ω values comes from the 2200ms^{-1} cross-section values (σ_o), and an improvement in these values could only be expected if some bare foil irradiations had been performed. However, the variances on the output values of $\left(\frac{G_r I_o}{g\sigma_o}\right)$ for all three isotopes are smaller than the corresponding input variances. This represents an improvement in the knowledge of these parameters.

These output values, however, should not be taken too seriously as improved estimates of the fundamental constants, $\frac{I_o}{g\sigma_o}$, because such a claim should only be made after including many careful measurements for a wider range of detector materials, into the consistency analysis. Despite the small sample size used, some information on the resonance

TABLE 5.2 Revised Input Data and Output Parameter Values for First Irradiation

Target	Parameter	Input Value	Output Value
-	α	-	$(1.22 \pm 5.1) \times 10^{-4}$
-	ϕ_e	-	$(1.301 \pm 0.024) \times 10^{6}$
-	χ^2/ν	-	2.23
^{197}Au	Ω	503.55 ± 0.72	503.57 ±0.72
^{55}Mn	Ω	242.1 ± 3.6	242.2 ±3.6
^{158}Gd	Ω	3.93 ± 0.79	3.93 ±0.80
^{197}Au	$\left(\frac{G_r I_o}{g\sigma_o}\right)$	6.03 ± 0.16	6.19 ±0.12
^{55}Mn	$\left(\frac{G_r I_o}{g\sigma_o}\right)$	0.976 ± 0.027	0.955±0.023
^{158}Gd	$\left(\frac{G_r I_o}{g\sigma_o}\right)$	46.9 ±18.0	44.7 ±10.6

TABLE 5.3 Revised Input Data and Output Parameter Values for Second Irradiation.

Target	Parameter	Input Value	Output Value
-	α	-	$(1.15 \pm 5.1) \times 10^{-4}$
-	ϕ_e	-	$(1.259 \pm 0.024) \times 10^{6}$
-	χ^2/ν	-	0.969
^{197}Au	Ω	503.55 ± 0.72	503.56 ±0.71
^{55}Mn	Ω	242.1 ± 3.6	242.15 ±3.4
^{158}Gd	Ω	3.93 ± 0.79	3.93 ±0.78
^{197}Au	$\left(\frac{G_r I_o}{g\sigma_o}\right)$	6.06 ± 0.16	6.15 ±0.12
^{55}Mn	$\left(\frac{G_r I_o}{g\sigma_o}\right)$	0.976 ± 0.027	0.963 ±0.022
^{158}Gd	$\left(\frac{G_r I_o}{g\sigma_o}\right)$	46.9 ± 18.0	45.2 ±10.1

integrals can be obtained if the individual variables in the parameter $\left(\frac{G_r I_o}{g\sigma_o}\right)$ are decoupled from one another.

This decoupling of the variables is quite complicated since the variables are tied together via the correlations and the correct method of error propagation must include the covariance terms.

For the data in this experiment, however, the appropriate covariance terms are either negligible or negative. An upper limit of the errors on the variables can be obtained, therefore, by treating the variables as independent and propagating the errors in the normal manner. The resonance integral values in Table 5.4 were obtained by taking the output $\left(\frac{G_r I_o}{g\sigma_o}\right)$ values from the consistency analysis and by using the input values for G_r, g and σ_o, removing the contributions due to these variables.

TABLE 5.4

Element	Estimate of I_o (barns)	Input value of I_o (barns)
^{197}Au	1582 ± 31	1549 ± 27
^{55}Mn	13.45 ± 0.33	13.70 ± 0.18
^{158}Gd	122 ± 32	127 ± 38

From Table 5.4, it can be seen that all of the estimates for I_o obtained from this work are consistent with the input values of I_o.

The value of $(I_o)_{^{158}Gd}$ obtained suggests that Steinnes' value (1975 is more reliable than the values cited in Gryntakis & Kim([10]. A study of the I_o values

for ^{55}Mn cited in Gryntakis & Kim shows that the estimate of I_o obtained in this work is inconsistent with three of the values.

[Baumann (1964): $I_o = 18.1 \pm 1.2$; Carre (1967): $I_o = 16.2 \pm 1.0$ and Gleason (1975): $I_o = 15.6 \pm 0.5$].

This suggests that more reliance should be put on the lower values of $(I_o)_{55_{Mn}}$ cited.

CHAPTER SIX

SUMMARY AND CONCLUSIONS

The model used in this work to relate the activity induced in a detector, in terms of nuclear cross-sections and neutron flux parameters, is based on the model described by Ahmad ([11] with slight modifications to allow for self-shielding effects.

In this model, the saturated γ-ray emission rate per unit mass of the target element is related to the flux parameters and the nuclear data as follows:

$$N_c = N_{AV}\,\theta P_\gamma\, M^{-1} g\sigma_o \left\{G_{th}\Phi_{th} + \phi_e \left[\frac{W'}{g} + f_1(\alpha) + \bar{E}_r^{-\alpha}\left(\frac{G_r I_o}{g\sigma_o} - f_2(0)\right) + f_2(\alpha)\right]\right\} \qquad - 6.1$$

If the detector is irradiated under cadmium cover, the equivalent model is:

$$(N_c)_{Cd} = N_{av}\,\theta P_\gamma M^{-1} g\sigma_o \phi_e \left\{\bar{E}_r^{-\alpha}\left(\frac{G_r I_o}{g\sigma_o} - f_2(0)\right) + f_2(\alpha)\right\} \qquad - 6.2$$

Using the procedure outlined in Chapter two, it is possible to determine γ-ray emission rates with a precision of around 1%, even for very small source-to-detector distances. (Note: If the absolute disintegration rate is measured instead of the γ-ray emission rate, then P_γ in equations 6.1 and 6.2 is set equal to 1).

The self-shielding factors can be calculated using a two-dimensional Monte-Carlo approach as described in Chapter Three. The agreement between calculated values and available literature values is very good.

In order to reduce any biases in the values for the flux parameters

obtained when solving equation 6.1 or 6.2, it is desirable to measure more isotopes than the minimum needed to determine these flux parameters. This produces an over-determined set of solutions which can be treated in a least-squares sense to find the "best-values". Since the nuclear data are also based on measurements, the least-squares minimization technique is also able to provide improved information on the nuclear data as a direct result of the experimental measurements.

The object of this work is to apply the described procedure, which does data testing, spectrum unfolding and data adjustment in one analysis, to experimental activation data obtained in the standard thermal and epithermal neutron spectrum facilities, at the National Physical Laboratory. When the consistency analysis was applied to the activation data obtained in the thermal flux facility, severe inconsistencies were found in the P_γ data for ^{116m1}In and ^{187}W. This led to a search for P_γ values for these isotopes which were consistent with the experimental measurements. The P_γ values for ^{116m1}In and ^{187}W which are consistent with the experimental data, are taken from refs 75 and 81 respectively. It should be noted that the P_γ value for the 417 keV transition in ^{116m1}In is significantly different from the value which is normally accepted, (Table of Isotopes ([75]), and shows that, contrary to the conclusions of Ahmad ([11]), not all of the P_γ values cited in the Table of Isotopes are reliable.

Although the uncertainties on the parameters ϕ_e and α could have been reduced further if more cadmium covered measurements had been performed; the output values for the flux parameters are in good agreement with the values obtained in an earlier measurement by Ryves and Paul (1968).

When the consistency analysis was applied to the activation data obtained in the epithermal flux facility, severe inconsistencies were found in the $\frac{G_r I_o}{g\sigma_o}$ values for ^{158}Gd when using the evaluated value of I_o.

This implies that some of the measurements included in the evaluation may not have been determined in an $\alpha = 0$ spectrum. Thus leading to a bias in the evaluated value. This consequently leads to the recommendation of Steinne's ([92] value for the resonance integral of ^{158}Gd. The most important result from this analysis is that the output values for α are both very small and consistent with zero. This is in agreement with the use of this facility as a slowing down neutron spectrum facility (i.e. $\alpha = 0$). Such a facility can be used for the fundamental determination of resonance integrals. It should be noted that more information on the nuclear data would be obtained if the data from both experiments were minimized simultaneously.

The success of this work provides further evidence in support of the model described by equations 6.1 and 6.2 and proves the suitability of the least-squares analysing technique. The ability of the consistency analysis to improve knowledge of nuclear data is evident. In conclusion, this work has provided new methods of treating some of the more difficult practical problems which arise in the calibration of neutron spectra and in the measurement of resonance activation cross-sections. The following points indicate where some improvements in the experimental and analytical procedures could be made.

a) For the best determination of the flux parameters, measurements of <u>both</u> bare and cadmium covered foils should be made for a set of isotopes which have a large spread in their effective resonance energy values.

b) The thinnest possible foils compatible with good counting statistics should be used, so as to reduce the self-shielding factors needed.

c) The Monte-Carlo code for calculating self-shielding factors could be improved by:

i) extending the two-dimensional approach to three dimensions so that edge effects can be considered.

ii) changing the Breit-Wigner formulae for multilevel formulae.

and iii) including the effect of Doppler broadening of the resonances.

It should be noted, that with a few alter-ations, the Monte-Carlo code could be used to calculate F_{Cd} factors.

d) The evaluation method described in Section 4.8.2 assumes that the resonance integrals are uncorrelated. This is not the case, since measurement of resonance integrals are usually made either relative to gold, colbalt or manganese as standards.
It the standard chosen and its numerical value used are known, then the appropriate covariance terms should be included.

e) In order to get direct information on I_o, using the techniques described in this work, it is important to be able to decouple the variable $\left(\frac{I_o}{g\sigma_o}\right)$, and propagate the errors correctly (i.e. take all the covariances into account). Work is presently being carried out on this problem by Gray ([93].

REFERENCES

1 C.H. Westcott, J. Nucl. Energy 2 (1955) 59.

2 R.W. Stoughton and J. Halperin, Nucl. Sci. Eng. 6 (1959) 100

3 O.T. Hogdahl, Radiochemical Methods of Analysis, I.A.E.A. Vienna, 1 (1965) 23.

4 M.M.R. Williams, The Slowing down and Termalization of Neutrons. North Holland (1966).

5 K.W. Geiger and L. Van der Zwan, Metrologia 2 (1966) 1.

6 T.B. Ryves and E.B. Paul, J. Nucl. Energy 22 (1968) 759.

7 T.B. Ryves, Metrologia 5 (1969) 119.

8 T. Bereznai and T.D. MacMahon, J. Radioanal.Chem. 45 (1978) 423.

9 F. De Corte, L. Moens, A. Simonits, A De Wispelaere and J. Hoste, J. Radioanal. Chem. 52 (1979) 295.

10 E.M. Gryntakis and J.I. Kim, NEA DATA BANK ND1540 (1980)

11 A. Ahmad, Ph.D. Thesis, University of London (1982)

12 K. Debertin and U. Schotzig, Nucl. Instr. & Meth. 140 (1977) 337.

13 W. Michaelis, Nucl. Instr. & Meth. 70 (1969) 253.

14 P. Quittner, Nucl. Instr. & Meth. 76 (1969) 115

15 R.G. Helmer and M.A. Lee, Nucl. Instr. & Meth. 178 (1980) 499. (and references quoted therein).

16 D.C. Robinson, Nucl. Instr. & Meth. 78 (1970) 120.

17 H.H. Jorch and J.L. Campbell, Nucl. Instr. & Meth 143 (1977) 551.

18 M. Dojo, Nucl. Instr. & Meth. 115 (1974) 425.

19 G.W. Phillips and K.W. Marlow, Nucl. Instr. & Meth. 137. (1976) 525.

20 H. Baba, S. Baba and T. Suzuki, Nucl. Instr. & Meth. 145 (1977) 517.

21 S.M. Jefferies, program LINE U.L.R.C. (1980).

22 J.T. Routti and S.G. Prussin, Nucl. Instr. & Meth. 76 (1969) 125.

23 L. Varnell and J. Trischuk, Nucl. Instr. & Meth, 76 (1969) 109.

24 C.M. Lederer, "Radioactivity in Nuclear Spectroscopy", J.H. Hamilton and J.C. Manthuruthil (editors); Gordon and Breach, New York (1972) p. 73 and references quoted therein.

25 L.A. McNelles and J.L. Campbell, Nucl. Instr. & Meth. 127 (1975) 73.

26 H.G. Balian and N.W. Eddy, Nucl. Instr. & Meth. 145 (1977) 389.

27 B.K. Barnes, Los Alamos Scientific Laboratory, Private Communication.

27 R.M. Parr, H. Houtermans and K. Schaerf, "Proceedings of the American Nuclear Society Topical Conference" at Mayaguez, Puerto Rico. CONF- 780421.

29 M. Wiernik, Nucl. Instr. & Meth. 95 (1971) 13 (and references quoted therein).

30 K. Huysmans, R. Gijbels and J. Hoste, J. Radioanal. Chem. 20 (1974) 51.

31 E. Junod, J. Radioanal Chem. 20 (1974) 113.

32 O.U. Anders, Nucl. Instr. & Meth. 68 (1969) 205.

33 H.H. Bolotin, M.G. Strauss and D.A. McClure, Nucl. Instr. & Meth. 83 (1970) 1.

34 E.J. Cohen, Nucl. Instr. & Meth. 121 (1974) 25.

35 M. Irfan and S.A. Husain, Nucl. Instr. & Meth. 143 (1977) 177.

36 L. Mortensen and J. Olsen, Nucl. Instr. & Meth. 113 (1973) 151

37 G. Azuelos, S.E. Crawford and J.E. Kitching, Nucl. Instr. & Meth. 117 (1974) 233.

38 D. Smith, National Physical Laboratory, Private Communication.

39 M. Wiernik, Nucl. Instr. & Meth. 96 (1971) 325.

40 I.A.E.A. Report G-2 (I.C.R.M. - Action 5/78 November 1978).

41 R.J. Gehrke, R.G. Helmer and R.C. Greenwood, Nucl. Instr. & Meth. 147 (1977) 405.

42 G.J. McCallum and G.E. Coote, Nucl. Instr. & Meth. 130 (1975) 189.

43 K. Debertin and U. Schotzig, Nucl. Instr. & Meth. 158 (1979) 471.

44 A. Luukko and P. Holmberg, Nucl. Instr. & Meth. 65 (1968) 121.

45 U. Schotzig, K. Debertin and K.F. Walz, Nucl. Instr. & Meth. 169 (1980) 43.

46 H.M. Weiss, Report on the International Comparison of gamma-ray reference sources (Jan 1982), Report B.I.P.M. - 82/1.

47 A. Ahmad and P.W. Gray, To be published.

48 L. Kokta, Nucl. Instr. & Meth. 112 (1973) 245

49 G.M. Roe, The Absorption of neutrons in Doppler Broadened Resonances. Rep KAPL-1241 (1954).

50 W.N. Selander, Theoretical Evaluation of Self-Shielding Factors due to scattering Resonances in Foils. Rep. AECL-1077 (1960).

51 N.P. Baumann, Resonance Integrals and Self-Shielding Factors for Detector Foils. Rep. DP-817 (1963).

52 N.P. Baumann and M.B. Stroud, Nucleonics 23 (1965) 98.

53 A.M. Judd, Nucl. Instr. & Meth. 23 (1963) 29.

54 P.F. Zweifel, Nucleonics 18 (1960) 174.

55 K.H. Beckurts and K. Wirtz, Neutron Physics, Springer Vergb, Berlin, (1964).

56 W.L. Zijp, Neutron Fluence Measurements. Tech. Rep. 107 (I.A.E.A. Vienna 1974).

57 M. Brose, Nukleonik 6 (1964) 134.

58 T.B. Ryves and K.J. Zieba, J. Phys. A : Math., Nucl. Gen 7 (1974) 2319.

59 E.J. Axton, J: Nucl. Energy Parts A/B 17 (1963) 125.

60 Y.A. Shreider, The Monte Carlo Method. International series of monographs in pure and applied mathematics, Vol 87 (1967) Pergamon Press.

62 W.H. Walker, C.H. Westcott and T.K. Alexander, Canad. J. Phys. 38 (1960). 57.

63 C.M. Jacks, A Study of Thermal and Resonance Flux Detectors Rep. DP-608 (1961).

64 R.H. Ritchie and H.B. Eldridge, Nucl. Sci. & Eng. 8 (1960). 300.

65 G.C. Hanna, Nucl. Sci. & Eng. 15 (1963) 325.

66 W.L. Zijp, Proceedings of the Fourth ASTM-EURATOM Symposium on Reactor Dosimetry (1982) CONF-820321 Vol 2 1221.

67 A. Ahmad, T.D. MacMahon, M. Macwani, M.J. Minski, J.G. Williams and T. Bereznai, Proceedings of 4th International Conference on Nuclear Methods in Environmental and Energy Research, CONF-800433 (1980).

68 H. Goldstein, J.A. Harvey, J.S. Story and C.H. Westcott, Recommended Definitions for Resonance Integral Cross-Sections, EANDC-12 (1961)

69 T.B. Ryves, National Physical Laboratory, Private Communication (1981).

70 P. Bode, M. De Bruin and P.J.M. Korthoven, J. Radioanal. Chem. 64 (1981) 153.

71 C. Segebade and H.P. Weiss, J. Radioanal. Chem. 45 (1978) 209.

72 Attix, Roesch and Tochilin, Radiation Dosimetry Vol I., Academic Press (1968).

73 Siegbahn, Alpha-Beta-and-Gamma-Ray Spectroscopy, Vol I North-Holland Publishing Company (1966).

74 E. Storm and H.I. Israel, Nuclear Data Tables A7 (1970) 565.

75 C.M. lederer and V.S. Shirley, Table of Isotopes 7th Edition. John Wiley & Sons (1978).

76 S.F. Mughabghab and D.I. Garber, Neutron Cross-Sections BNL-325 3rd Edition, Vol. 1, New York (1973).

77 L. Moens, F. De Corte, A. Simonits, A. De Wispelaere and J. Hoste, J. Radioanal. Chem. 52 (1979) 379.

78 R.C. Weast, Handbook of Chemistry and Physics, 57th Edition, CRC Press (1977).

79 E.M. Gryntakis and J.I. Kim, NEA Data Bank, ND1540 (1980)

80 W.L. Zijp and J.H. Baard, Nuclear Data Guide for Reactor Neutron Metrology, Part I ECN-70 (1979).

81 D.S. Brenner and R.A. Meyer, Phys. Rev. C, 13 (1976) 1288.

82 F. De Corte, A. Simonits, L. Moens, A. De Wispelaere and J. Hoste, INW/KFKI Interim Report (Sept. 1982).

83 W. Taylor, U.K.A.E.A., A.E.E. Winfrith, Private Communication (Sept. 1982).

84 F. De Corte, K. Sordo-el Hammami, et al., J. Radioanal. Chem. 62 (1981) 209.

85 P.J. Campion, J. Applied Radiation and Isotopes 4 (1959) 232.

86 A.P. Baerg, Metrologia 2 (1966) 23.

87 J.B. Olomo, Ph.D. Thesis, University of London (1979)

88 A.P. Baerg, Nucl. Instr. & Meth. 112 (1973) 143.

89 T. El Nimr, F. De Corte, L. Moens, A. Simonits and J. Hoste, J. Radioanal. Chem. 67 (1981) 421.

90 Yuan Han-rang, International Conference for Nuclear Data for Science and Technology (Sept. 1982) Antwerp

91 J.G. Williams, University of London (1982) Private Communication.

92 E. Steinnes, J. Inorg, Nucl. Chem. 37 (1975) 1591

93 P.W. Gray, U.L.R.C., University of London.

Appendix I

The calculation of the angles through which the neutron is scattered and its change of energy in the thermal self-shielding problem, was done as follows (see Fig. A.1).

Let the velocities of the incident neutron and scattering atom be given by v_1 and v_2 respectively.

where $v_1 = v_1 \{\sin\theta_1 i + \cos\theta_1 k\}$

and $v_2 = v_2 \{\sin\theta_2 \cos\psi_1 i + \sin\theta_2 \sin\psi_1 j + \cos\theta_2 k\}$

where i, j and k are unit vectors along the x, y and z-axes resp.

Fig. A.1

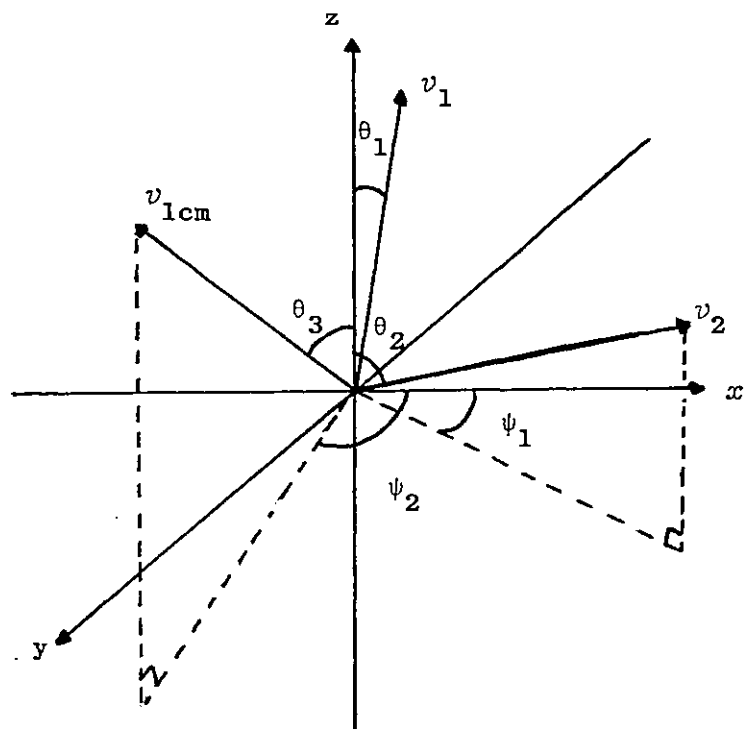

then $v_{rel} = v_1 - v_2 = (v_1\sin\theta_1 - v_2 \sin\theta_2 \cos\psi_2) i$

$+ (-v_2\sin\theta_2 \sin\psi_1)\, j$

$+ (v_1\cos\theta_1 - v_2 \cos\theta_2) k$

and $v_{cm} = \frac{m_1}{m_1+m_2} v_1 + \frac{m_2}{m_1+m_2} v_2$

where v_{rel} is the relative velocity of the two particles and v_{cm} is the centre of mass velocity.

For a neutron incident on an atom, assume $m_1 = 1$ and $m_2 = A$ where A is the atomic weight of the scattering element.

Then

$$v_{cm} = \frac{1}{(A+1)} \{(v_1 \sin\theta_1 + v_2 A \sin\theta_2 \cos\psi_1)i + (v_2 A \sin\theta_2 \sin\psi_1)j + (v_1 \cos\theta_1 + v_2 A \cos\theta_2)k\}$$

In the centre of mass system, the neutron has velocity v_{1cm} before the collision where $v_{1cm} = v_1 - v_{cm}$

i.e.

$$v_{1cm} = \frac{A}{1+A} v_{rel}$$

If scattering is isotropic in the centre of mass system then; after collision, if angles of scattering are given by θ_4 and ψ_3 then direction and velocity of neutron is given by:

$$v'_{1cm} = |v_{1cm}| \{\sin\theta_4 \cos\psi_3 i + \sin\theta_4 \sin\theta_3 j + \cos\psi_4 k\}$$

After scattering, velocity of neutron in lab frame is given by

$v'_1 = v'_{1cm} + v_{cm}$

i.e. $v'_1 = (|v_{1cm}| (\sin\theta_4 \cos\psi_3) + \frac{1}{(A+1)} (v_1 \sin\theta_1 + v_2 A \sin\theta_2 \cos\psi_1)i$

$$+ (|v_{1cm}| \sin\theta_4 \sin\psi_3 + \frac{1}{(A+1)} (v_2 A \sin\theta_2 \sin\psi_1))j$$

$$+ (|v_{1cm}| \cos\theta_4 + \frac{1}{(A+1)} (v_1 \cos\theta_1 + v_2 A \cos\theta_2))k$$

The projection on the z-axis is given by $v_1' \cdot k$

i.e. $\cos\theta' = \dfrac{v_1' \cdot k}{|v_1'||k|}$

$$\cos\theta' = \frac{v_{1cm}\ \cos\theta_4 + \frac{1}{A+1}\ (v_1\ \cos\theta_1 + v_2 A \cos\theta_2)}{|v_1'|}$$

and the speed of the neutron is given by $|v_1'|$.

Appendix II

Variance-Covariance Information for Graphite-Pile Experiment

A complete statement of the uncertainties in the parameters is given by its covariance matrix and is needed for the computation of the uncertainties in any function of the data. A more useful way of looking at the covariances is to transform the covariance matrix in terms of the standard deviations and the correlation matrix. The standard deviations are the square root of the diagonal elements of the covariance matrix and the correlation matrix is just:

$$\rho(x,y) = \frac{\mathrm{cov}(x,y)}{\Delta x \cdot \Delta y}$$

where x and y are the parameters and Δx, Δy are their respective standard deviations. It is the usual convention to present the standard deviations together with the parameter values as shown in Tables A.2.2 and A.2.3.

The diagonal elements of the correlation matrix are therefore always unity, and the off-diagonal elements must be in the range -1 to +1. The term correlation coefficient is a measure of the tendency for x and y to be linearly related.

The $\rho(x,y)$ matrix for the Graphite-Pile experiment is (34 x 34) in dimensions.

However, since the correlations in the parameters 21 to 34 are negligible, only the correlations for the first 20 parameters are listed in Tables A.2.2 and A.2.3.

TABLE A.2.1 Parameter Numbers

Parameter number	Parameter	Element
1	α	-
2	Φ_{th}	-
3	ϕ_e	-
4	$\eta(412)$	Gold
5	$\eta(847)$	Manganese
6	$\eta(1039)$	Copper
7	$\eta(138)$	Indium
8	$\eta(417)$	
9	$\eta(819)$	
10	$\eta(1097)$	
11	$\eta(1293)$	
12	$\eta(1507)$	
13	$\eta(479)$	Tungsten
14	$\eta(511)$	
15	$\eta(618)$	
16	$\eta(625)$	
17	$\eta(685)$	
18	$\eta(772)$	
19	$\eta(1368)$	Sodium
20	$\eta(58)$	Colbalt

TABLE A.2.2 Correlation Matrix for Graphite-Pile Experiment

Parameter number	1	2	3	4	5	6	7	8	9	10
1	1.0									
2	.047	1.0								
3	-.562	-.13	1.0							
4	.01	-.17	-.096	1.0						
5	.044	.496	-.012	-.094	1.0					
6	-.008	-.173	.014	.031	-.087	1.0				
7	.052	-.445	-.086	.094	-.229	.078	1.0			
8	.059	-.502	-.097	.106	-.258	.088	.253	1.0		
9	.056	-.481	-.094	.101	-.248	.085	.243	.274	1.0	
10	.065	-.556	-.107	.117	-.286	.098	.280	.316	.303	1.0
11	.050	-.427	-.083	.090	-.220	.075	.215	.243	.233	.269
12	.030	-.252	-.049	.053	-.130	.044	.127	.143	.138	.159
13	-.043	-.495	-.020	.099	-.255	.087	.233	.263	.253	.292
14	-.040	-.459	-.019	.092	-.236	.081	.217	.244	.234	.270
15	-.050	-.582	-.023	.117	-.300	.102	.274	.310	.297	.343
16	-.048	-.561	-.022	.113	-.289	.099	.265	.299	.286	.331
17	-.050	-.582	-.023	.117	-.300	.102	.274	.309	.297	.343
18	-.051	-.589	-.023	.118	-.304	.104	.278	.313	.301	.347
19	-.005	-.228	.018	.040	-.114	.040	.103	.116	.112	.129
20	-.024	-.455	.032	.082	-.228	.079	.207	.233	.224	.258

TABLE A.2.3 Correlation Matrix for Graphite-Pile Experiment

Parameter number	11	12	13	14	15	16	17	18	19	20
1										
2										
3										
4										
5										
6										
7										
8										
9										
10										
11	1.0									
12	.122	1.0								
13	.224	.132	1.0							
14	.208	.123	.250	1.0						
15	.263	.156	.317	.294	1.0					
16	.254	.150	.305	.283	.360	1.0				
17	.263	.156	.317	.293	.373	.359	1.0			
18	.267	.158	.321	.297	.378	.364	.378	1.0		
19	.099	.058	.114	.106	.134	.129	.134	.136	1.0	
20	.199	.117	.229	.213	.270	.260	.270	.273	.104	1.0

The usefulness of the correlation comes in when calculating the uncertainties of a function of two or more parameters which are correlated. It is misleading to propagate the error in that function simply by considering their variances. The correct method of propagation must include the covariance terms.